LUNDS UNIVERSITET

KBTM01

Degree Project in Biotechnology

An Exploration of Siderophore Production in Bacterial Isolates from Icelandic Hot Springs

---

Emilie Grøntveit Tverå

Supervisor:

Roya R. R. Sardari

Examiner:

Eva Nordberg Karlsson

Date of submission: 27.05.2025

Abstract

Thermophilic microorganisms represent a promising but underexplored source of thermostable siderophores—iron-chelating metabolites with potential applications in bioremediation, agriculture, and medicine. This study investigated three thermophilic bacterial strains isolated from Icelandic hot springs for their ability to produce siderophores under iron-limited conditions. Fermentations were carried out at 60–65°C in media with varied iron availability, including supplementation with 100 μM 2,2'-dipyridyl (DIP) to induce iron stress. Growth was monitored spectrophotometrically, and siderophore production was assessed using a panel of chemical assays, including the Chrome Azurol S (CAS) test and class-specific detection methods (Arnow, Rioux, Csaky, Atkin, and Tetrazolium). Statistical significance was determined at $\alpha = 0.05$.

Strain 4624 demonstrated robust growth and produced significant quantities of catecholate siderophores in DIP medium, with strong signals observed in both Arnow ($p < 0.001$) and Rioux assays. Hydroxamate production was also suggested by Csaky results ($p = 0.044$), though assay instability warrants caution. In contrast, strain 7349 showed only weak trends toward hydroxamate activity, while strain 623 exhibited neither siderophore production nor growth resilience under iron stress. Partial purification of catecholates from strain 4624 using XAD-2 resin confirmed enrichment, though recovery was limited due to early saturation.

These findings validate earlier genomic predictions and highlight the potential of geothermal bacteria, particularly strain 4624, as sources of siderophores operable at high temperatures. Further optimisation of culture conditions and downstream purification could advance their use in industrial or environmental applications.

Acknowledgements

First and foremost, I would like to thank my supervisor Roya. Her belief in my abilities and talent meant a great deal and was a major source of motivation throughout this project. Having someone to bounce ideas off and troubleshoot problems with offered valuable perspective, and her presence made the process lighter, whether we were working or simply chatting. I am also grateful to Eva, my examiner, for allowing me to take on this exciting project, and to Matís for providing the bacterial strains and conducting the genetic screening, which helped guide the experimental choices. During the course of the project, I received much-needed support from the Fermentation Research Group, to whom I extend my gratitude. The members were generous with their time and knowledge, helping me find my footing in the lab.

The biggest thanks in my heart, though, go to my friends: Nina, Laura, Mikael, Anna, Lovro, and Renée. You created the warm, vibrant space around me that I needed to stay grounded and energised. Between all the conversations, spontaneous plans, and adventures we shared, you brought so much joy into this chapter of my life. I couldn't have asked for a better group of people to have around.
To my parents, thank you for your endless support and unwavering belief in me. You have always stood behind me in all my decisions, and knowing I could rely on your love and encouragement has meant everything to me.

Lastly, to my partner Saeid. You have been my constant throughout this journey, standing by me in both the good days and the difficult ones. You've always known exactly when I needed someone to listen, when I needed comfort, and when I needed a little push forward. Your quiet strength, patience, and care have carried me through more than I can say.
Takk for at du alltid har vært i hjørnet mitt. Jeg er så takknemlig for at jeg har deg ved min side.

Looking back, I feel proud. This has been a significant undertaking, and having carried it through on my own terms, I leave this chapter with a strong sense of accomplishment.

Contents

1 Introduction

Meeting the United Nations Sustainable Development Goals and impending decarbonisation targets requires a decisive shift from petroleum based supply chains to biological routes for production of fuels, materials and high-value metabolites (Del Hierro et al., 2024). Biotechnology has emerged as a critical enabler of this transition, with recent assessments highlighting its potential to address numerous sustainability challenges. However, current industrial pipelines continue to exploit only a small fraction of microbial diversity (Crowther et al., 2024; Warchold and Pradhan, 2025; Pandey et al., 2024).

Extremophiles, particularly thermophiles, represent a largely untapped reservoir of robust microbial hosts and thermostable enzymes capable of withstanding industrial stresses such as elevated temperatures, salinity, and extreme pH (Zheng et al., 2025). Exploiting these traits can reduce contamination risks, enable in situ product recovery, and open new avenues for biosynthesis. In addition to their primary metabolic capabilities, thermophilic microorganisms are gaining attention as a promising yet under-explored source of secondary metabolites with novel structures and bioactivities. Studies on hot-spring *Bacillus* strains and recent reviews of thermophilic fungi highlight the diversity and pharmaceutical potential of these compounds (Fandi et al., 2024; Pushparaj et al., 2023). Thermophilic strains have already shown promise in processes such as lignocellulose degradation, bio-hydrogen production, and polyhydroxyalkanoate synthesis at temperatures exceeding 60°C, offering advantages including reduced sterilisation costs and shorter reaction times (Gallo et al., 2024). Operating bioprocesses at thermophilic conditions also accelerates enzymatic turnover and lowers or eliminates cooling demands, ultimately enhancing process efficiency and reducing costs (Sitara et al., 2024; Pattanakittivorakul et al., 2024).

Siderophores are ferric iron-chelating compounds secreted by microbes to survive in iron-limited environments, a strategy widely observed among both bacteria and fungi (Kumar et al., 2024; Choi et al., 2024). These biomolecules have inspired a broad range of technological applications. In medicine, siderophore–drug conjugates and inhibitors of siderophore biosynthesis are under investigation as strategies to combat antimicrobial resistance (Gräff and Barry, 2024;

Rocha et al., 2025). Siderophores are also being explored as a therapeutic approach to treat iron overload in patients with transfusion-dependent anaemia (Albelda-Berenguer et al., 2019). In agriculture, siderophore-producing *rhizobacteria* act as environmentally friendly biocontrol agents by depriving plant pathogens of iron (Deb and Tatung, 2024).

Iceland's geothermal fields combine extreme heat with unique pH- and mineral profiles, driving the evolution of distinctive thermophilic strains (Burkhardt et al., 2024). Discoveries such as the ethanologenic *Thermoanaerobacter thermohydrosulfuricus* strain AK152 from Grensdalur highlight how these hot springs can yield novel organisms of clear biotechnological promise (Abraham et al., 2024). Matís, a government-owned independent research company in Iceland, has isolated a range of thermophilic strains from local geothermal sites with the aim of assessing their biotechnological potential. Preliminary characterisation involved AntiSMASH analysis, a tool used to identify secondary metabolite biosynthetic gene clusters in bacterial genomes (Medema et al., 2011), alongside CAS-based (Chrome azurol S) assays to detect siderophore (Shin et al., 2001). Among the isolates, three strains, 7349, 4624, and 623, exhibited particularly promising indications of siderophore activity.

This thesis builds upon those findings by further investigating the siderophore-producing potential of the three strains. The work involved cultivating the bacteria under varying iron concentrations to identify conditions most favourable for siderophore production, applying chemical assays to indicate the likely siderophore type, and, where feasible, attempting partial purification to gain further insight into the nature of the compounds. While exploratory in scope, the findings support ongoing efforts to identify thermophilic strains with traits suited for more sustainable and resilient bio-production systems, including the microbial synthesis of siderophores with potential industrial relevance.

2 Literature Study

This section provides an overview of the scientific concepts relevant to the project, including iron availability and uptake, siderophore chemistry, thermophilic bacteria, and the analytical methods used for siderophore detection. Together, these topics form the foundation for understanding the rationale and design of the experimental work.

2.1 Iron Availability and Microbial Iron Uptake

Iron is the red thread that stitches together core microbial processes. Its heme and iron–sulphur cofactors sit at the heart of cytochromes for respiration, nitrogenases for nitrogen fixation, ribonucleotide reductases for DNA synthesis, and dozens of redox and radical enzymes(Kümpel et al., 2024). Iron's biochemical value stems from its redox versatility. It easily cycles between the ferrous (Fe^{2+}) and ferric (Fe^{3+}) states, making it ideal for catalytic roles. EcoCyc, a curated Escherichia coli database, annotates over 240 iron-binding proteins, spanning the respiratory chain and key systems like ribonucleotide reductase (Keseler et al., 2017). Loss-of-function studies show that when intracellular iron levels fall below $\approx$2 μM, energy generation stalls, ATP production declines, and oxidative-stress defences collapse, ultimately halting microbial growth (Gao and Span, 2025; Baez et al., 2022).

Yet paradoxically, bioavailable iron is scarce in many microbial habitats. Although ferrous iron (Fe^{2+}) is relatively soluble under anaerobic or acidic conditions ($\sim$0.1 M at pH 7.0), it oxidises rapidly to Fe^{3+} in the presence of oxygen (Andrews et al., 2003). Ferric iron, in turn, hydrolyses and precipitates at neutral pH, reducing its solubility to $\sim 10^{-18}$ M, twelve orders of magnitude below cellular demand (Cain and Smith, 2021; LeBlanc and Wuest, 2024; Schaible and Kaufmann, 2004). This scarcity has driven the evolution of specialised iron acquisition systems. To overcome this limitation, many bacteria and fungi secrete siderophores. Which are small, high-affinity chelators that scavenge Fe^{3+} from the environment and ferry it back to the cell (Kumar et al., 2024). These systems are especially important in aerobic, neutral-pH environments where ferric iron dominates but is largely insoluble.

Because iron is often the limiting resource in microbial ecosystems, competition for it has

shaped complex community interactions. A common strategy is siderophore piracy, where a cell expresses receptors for siderophores it does not produce, allowing it to import iron without paying the biosynthetic cost (Sexton et al., 2017). This behaviour contributes to what some authors describe as the "iron-net"—a dynamic network in which siderophores act as shared currency and microbes adopt roles as producers, cheaters, or both (Gu et al., 2025). The diversity of uptake, storage, and regulatory strategies evolved around iron reflects its deep influence on microbial evolution. It has shaped physiology, behaviour, and ecological interactions, with siderophores representing just one part of a much larger adaptive landscape.

2.2 Siderophores

Siderophores are low-molecular-weight, high-affinity chelators produced by bacteria, fungi, and graminaceous plants to acquire ferric iron (Fe^{3+}) from the environment. Typically ranging between 500–1500 Da in size, these molecules are synthesised and secreted in response to iron limitation, and their primary biological function is to ferry Fe^{3+} into microbial cells (Hider and Kong, 2010). While their principal role is in iron acquisition, siderophores have also been shown to bind other trace metals, including molybdenum, manganese, cobalt, and nickel, potentially making them available for microbial uptake under specific conditions (Braud et al., 2009; Bellenger et al., 2008).

When iron becomes limiting, bacteria activate specialised gene clusters that control siderophore production. These molecules are synthesised in the cytoplasm and must be secreted to function. In the model organism *E. coli*, this process is carried out by two transporters: the inner-membrane pump EntS exports the siderophore to the periplasm, while the outer-membrane protein TolC completes the secretion to the extracellular space (Bleuel et al., 2005). Secretion is essential, as the siderophore must access the surrounding environment to chelate Fe^{3+}, without export, high-affinity iron uptake cannot proceed (Miethke and Marahiel, 2007). Once a siderophore has bound iron, the resulting ferric complex is recognised and taken up by specific receptors. In Gram-negative bacteria, this begins with a TonB-dependent receptor in the outer membrane, which binds the complex and uses energy from the TonB–ExbBD motor (anchored in the inner membrane) to translocate it into the periplasm (Silale and van den Berg, 2023).

From there, a siderophore binding protein (SBP) shuttles the complex to an ATP-binding cassette (ABC) transporter, which imports it into the cytoplasm. (Hu and Zheng, 2021; Tsylents et al., 2024). Finally, intracellular enzymes, usually esterases or reductases, release Fe^{2+} from the complex, completing siderophore cycle (Miethke and Marahiel, 2007).

2.2.1 Classification and structure

Siderophores are typically grouped into three major families based on the chemical nature of their iron-binding functional groups: catecholates, hydroxamates, and carboxylates (Winkelmann, 1991). While all siderophores serve the same core purpose—solubilising and delivering Fe^{3+} to the cell—their structural diversity reflects adaptation to different environmental conditions and biosynthetic strategies. To date, over 500 distinct siderophores have been described, with approximately 270 structurally characterised (Hider and Kong, 2010). Among these, catecholate-type siderophores are the most prevalent in bacteria, followed by hydroxamates and carboxylates (Ahmed and Holmström, 2014). There are also mixed-type siderophores that incorporate two or more donor chemistries within the same scaffold, often giving pathogens an edge in overcoming host defence systems (Hider and Kong, 2010). The binding group of each siderophore family can be seen in Figure 1.

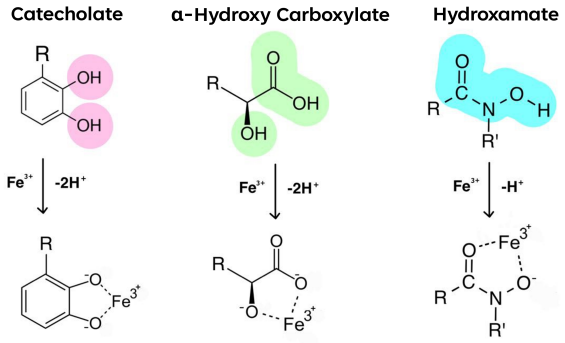

Figure 1: Representative functional groups involved in Fe^{3+} binding for the three major siderophore classes: catecholates, α-hydroxy carboxylates, and hydroxamates. The coordinating atoms are highlighted for each class, showing the typical bidentate interaction with ferric iron. Catecholates bind via two adjacent hydroxyl groups on an aromatic ring, α-hydroxy carboxylates through a hydroxyl and carboxyl group on a central carbon, and hydroxamates through an adjacent carbonyl and hydroxylamine oxygen.

Catecholates are one of the three principal siderophore families, characterised by the use of 2,3-dihydroxybenzoyl (a benzene ring with two neighbouring hydroxyl groups) to chelate Fe^{3+}. The class was first recognised in 1958, when *Bacillus subtilis* was found to secrete a glycine conjugate of 2,3-dihydroxybenzoic acid under iron-limited conditions (Ito and Neilands, 1958). Catecholate siderophores are especially common in Gram-negative bacteria, such as *Escherichia coli* and *Salmonella enterica*, but also occur in some Gram-positive genera like *Bacillus* (Hider and Kong, 2010). Their exceptional affinity for Fe^{3+} arises from the catechol groups, each of which donates two oxygen atoms to coordinate the iron ion. A well-studied example is enterobactin, synthesised by many Enterobacteriaceae, which features three catechol units arranged on a small cyclic backbone. This compact, hexadentate structure forms an extremely stable complex with Fe^{3+}, reflected in its formation constant (log K ∼52), the highest known for any natural chelator (Raymond et al., 2003). By comparison, most hydroxamate and carboxylate systems plateau near log K ∼30–40 (Ahmed and Holmström, 2014). Catecholate siderophores typically exhibit pKa values around 6.5 and 11.5 (Miethke and Marahiel, 2007), and their iron-binding capacity is highly pH-dependent. Binding does not involve a redox reaction, Fe^{3+} remains in its oxidised form, but requires deprotonation of the catechol hydroxyl groups. This occurs more readily at neutral or slightly basic pH, whereas at lower pH, proton competition weakens complex formation (Miethke and Marahiel, 2007; Ahmed and Holmström, 2014). Consequently, catecholate siderophores function most effectively in neutral environments.

Hydroxamates form the second major class of siderophores, defined by their use of hydroxamate groups (–C(=O)N(OH)R) to coordinate Fe^{3+}. Iron binding occurs through both the carbonyl oxygen and the deprotonated N–O^- oxygen (Hider and Kong, 2010). Typical hydroxamate siderophores, such as ferrichrome and desferrioxamine B, coordinate iron in a hexadentate fashion using three hydroxamate units, yielding formation constants in the range of log K ∼29–31. Though weaker than catecholates, this affinity still exceeds that of synthetic chelators like EDTA. (Hider and Kong, 2010; Himpsl and Mobley, 2019). Hydroxamates are produced by a range of microbes, including many filamentous fungi (e.g., *Aspergillus*) and several actinobacterial species (Hider and Kong, 2010). Hydroxamate siderophores show optimal iron-binding activity between pH 6–8, while below pH 5 protonation of the N–O^- donor group

significantly reduces binding affinity (Hider and Kong, 2010).

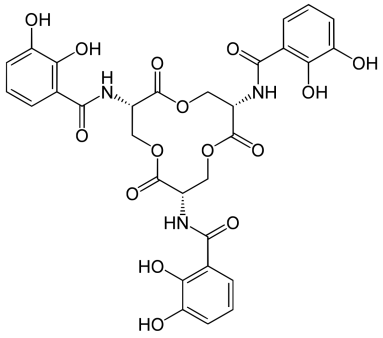

(a) Enterobactin, a catechol.

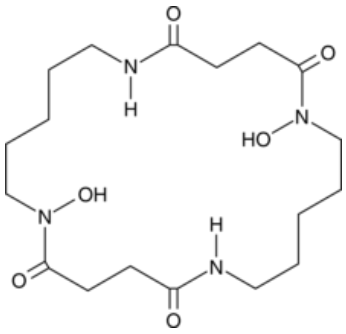

(b) Bisucaberin, a hydroxamate.

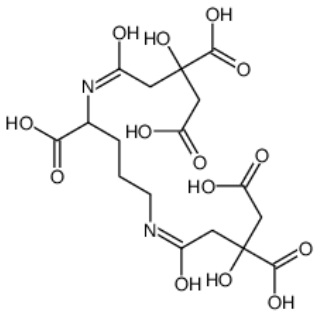

(c) Staphyloferrin A, a carboxylate.

Figure 2: Examples of siderophores from the three classes.

Carboxylates form the third major siderophore class and are defined by their use of carboxylate ($–COO^-$) groups, often in combination with adjacent α-hydroxy groups, to coordinate Fe^{3+} (Hider and Kong, 2010). These α-hydroxy-carboxylate motifs bind iron through both the hydroxyl and carbonyl oxygens, typically forming hexadentate complexes with overall affinity constants ranging from log K ∼24–32, substantially lower than those of catecholates and hydroxamates (Hider and Kong, 2010; Himpsl and Mobley, 2019). Their binding affinity peaks around neutral pH but remains relatively effective under mildly acidic conditions, as carboxylic acids deprotonate more readily than catechol groups (Miethke and Marahiel, 2007). A classic example is staphyloferrin A, produced by *Staphylococcus*, which also binds iron in a hexadentate manner (Konetschny-Rapp et al., 1990). Notably, more than half of marine siderophores are carboxylates, many of which exhibit photoreactivity. This unique mechanism triggers decarboxylation of the Fe^{3+} complex upon sunlight exposure, reducing it to Fe^{2+} and

promoting iron release in sunlit surface waters (Butler and Theisen, 2010; Vraspir and Butler, 2009). This built-in photochemical mechanism is thought to aid iron bioavailability in marine ecosystems.

Structurally, siderophores are highly diverse, with no single conserved scaffold. Many are peptide-based and assembled by non-ribosomal peptide synthetases (NRPSs). For instance, enterobactin has a cyclic backbone of three serine residues linked to catechol arms (Raymond et al., 2003), while ferrichrome features a cyclic hexapeptide of alternating hydroxamate donors and small amino acids (Jenner et al., 2023). In contrast, NRPS-independent (NIS) siderophores lack a peptide backbone and are built from citrate or polyamine cores, as seen in petrobactin and desferrioxamine (Bailey et al., 2018; Manck et al., 2022; Miethke and Marahiel, 2007).

This structural and chemical diversity allows microbes to adapt their iron acquisition strategies to different environmental conditions, ecological niches, and levels of competition, demonstrating how central iron is to microbial survival and evolution.

2.2.2 Applications of Siderophores

Advances in biotechnology have enabled the large-scale production, isolation, and modification of siderophores, opening the door to a range of industrial and biomedical applications. Their natural ability to scavenge iron, and in some cases, other metal ions, has been harnessed to address diverse global challenges.

One of the most urgent challenges is antimicrobial resistance (AMR), which was associated with an estimated 4.95 million deaths in 2019 alone (Murray et al., 2022). Many pathogens, including *Escherichia coli*, *Staphylococcus aureus*, and *Klebsiella pneumoniae*, survive in the iron-limited environment of the host by producing siderophores (Skaar, 2010). This natural strategy has inspired therapeutic innovations such as sideromycin antibiotics, where a siderophore is chemically linked to an antibiotic molecule. The conjugate is actively imported by susceptible bacteria under iron starvation, releasing the antibiotic inside the cytoplasm, an approach often likened to a "Trojan horse" (Wang et al., 2022a). Some pathogens produce their own sideromycins while simultaneously expressing immunity genes to evade their

toxic effects. Biomedical researchers have begun to replicate this mechanism, linking approved drugs to siderophores to selectively target AMR pathogens. One such example, cefiderocol, was approved for clinical use in 2019 (Gräff and Barry, 2024).

In another medical context, the hydroxamate desferrioxamine forms the basis of Desferal, a drug used to treat iron overload in patients with transfusion-dependent anaemia (Albelda-Berenguer et al., 2019). Meanwhile in agriculture, siderophore-producing rhizobacteria serve as environmentally friendly biocontrol agents. By depriving soil-borne pathogens of iron, these bacteria help protect crops without relying on chemical pesticides (Deb and Tatung, 2024). This offers a promising route to more sustainable farming practices.

Siderophores have also shown promise in environmental remediation. For example, siderophores from *Pseudomonas azotoformans* were able to leach 92% of arsenic from contaminated soils (Nair et al., 2007). Other studies have demonstrated the removal of heavy metals such as Cd^{2+}, Pb^{2+}, Hg^{2+}, and Ni^{2+} from contaminated soils using mixed-type siderophores, with removal efficiencies ranging from 52.9–83.6% (Yi et al., 2022). Beyond one-off treatments, immobilised siderophores are being explored for use in continuous flow systems, potentially enabling scalable and recyclable metal recovery processes (Hofmann et al., 2021).

Taken together, these examples highlight the versatility of siderophores as tools for solving problems across medicine, agriculture, and environmental engineering. Their unique chemistry, combined with expanding biotechnological control over their production, positions them as promising agents for sustainable innovation across multiple sectors.

2.3 Thermophilic Microorganisms

Thermophilic bacteria are defined by their ability to grow at elevated temperatures, typically between 40 and 90°C, with optimal growth commonly occurring between 55 and 65°C (Featherstone, 2015). These organisms naturally inhabit high-temperature environments such as deep-sea hydrothermal vents, volcanic regions, compost heaps, and especially hot springs (Panda et al., 2019)

A range of molecular adaptations has allowed these bacteria to persist under such extreme conditions. Thermostable enzymes and proteins resistant to denaturation and proteolysis, membranes enriched with saturated fatty acids to maintain integrity, genomic DNA stabilised by positive supercoiling, and chaperonins that assist in refolding damaged proteins are among some of these adaptions (Haki and Rakshit, 2003). These adaptations also confer significant biotechnological advantages. Thermophiles often exhibit higher metabolic rates and produce enzymes that are both chemically and physically stable under harsh industrial conditions (Mehta et al., 2016). As a result, thermophilic enzymes have been widely adopted in biotechnology, particularly in processes involving high temperatures, extreme pH values, or the presence of solvents. For example, highly thermostable α-amylases have been isolated from *Thermus* and *Bacillus* species found in hot springs, demonstrating remarkable catalytic performance at elevated temperatures (Shaw et al., 1995; Mamo et al., 1999).

Iceland's geothermal fields offer a particularly rich source of thermophiles due to their wide range of temperatures, pH values, and mineral profiles. Environmental surveys from hot springs in regions such as Torfajökull have recorded temperatures from 45°C up to 100°C, often in alkaline waters with pH 8–8.5 (Podar et al., 2020). These varied habitats support diverse microbial communities, with dominant phyla at 50–65°C including Cyanobacteria, Chloroflexi, and Bacteroidetes. Icelandic hot springs have yielded several noteworthy thermophiles of scientific and industrial interest. For instance, *Thermus islandicus* sp. nov., isolated from the Torfajökull geothermal area, grows optimally at 65°C and pH 6–7 and demonstrates sulfur-oxidising activity stable up to 79°C (Bjornsdottir et al., 2009). Another example is the acidophilic archaeon *Sulfolobus islandicus*, which thrives at 75–85°C and pH 2–3 and contains extensive genetic diversity across CRISPR/Cas and metabolic modules (Guo et al., 2011).

2.3.1 Siderophores from Thermophiles

Despite the well-documented potential of thermophiles for industrial enzyme production, relatively few siderophores have been characterised from thermophilic organisms. Nevertheless, a few noteworthy examples have been reported, offering a glimpse into their biotechnologi-

cal promise. *Parageobacillus* sp. KH3-4, a thermophilic Bacillaceae strain with an optimal growth temperature of 65°C, was recently shown to produce bacillibactin. Interestingly, the non-ribosomal peptide synthetase (NRPS) enzymes responsible for its biosynthesis remained active at temperatures ≥60°C, and the Fe-bacillibactin complex retained high binding affinity across a broad 30–70°C range (Izumi et al., 2025). These features suggest a potential role for thermophilic siderophores in processes such as high-temperature bioremediation or metal recovery under harsh industrial conditions.

While this examples demonstrate that thermophiles can produce thermotolerant siderophores, their overall chemical diversity remains poorly explored. Available evidence suggests that such siderophores often function across broader temperature and pH ranges than those from mesophilic species, making them particularly attractive for industrial applications such as metal extraction, environmental remediation, and high-temperature fermentation (De Serrano et al., 2016). Given the limited number of characterised siderophores from thermophilic microbes, expanding screening efforts to include extremophiles is a key step toward unlocking their full biosynthetic potential.

2.4 Fermentation Conditions and Iron Regulation

Siderophore production in bacteria is tightly regulated by environmental iron availability. Under low-iron conditions, bacteria increase siderophore output to improve iron uptake, a response that can be deliberately induced in laboratory cultures for screening purposes (McHugh et al., 2003).

The most commonly used strategy involves limiting bioavailable iron in the growth medium, either by omitting added iron altogether or by actively removing free iron through the addition of synthetic chelators (Southwell et al., 2024). Defined minimal media with no added iron can produce iron-limiting conditions, but in practice, trace contamination or residual iron in components may still allow sufficient availability to suppress siderophore production (Nudel et al., 2001). For this reason, iron chelators such as 2,2'-dipyridyl (DIP), also known as 2,2'-bipyridyl or bpy, are often employed. DIP selectively binds Fe^{2+}, creating iron-deficient conditions that

closely mimic those encountered by pathogens in host environments (Southwell et al., 2024). Its addition has been shown to reliably induce siderophore production across various bacterial species, including *E. coli* and *Stenotrophomonas maltophilia*, where DIP triggers the expression of genes involved in biosynthesis of enterobactin and hydroxamate type siderophore (McHugh et al., 2003; Nas and Cianciotto, 2017). Experimental optimisation studies have confirmed the effectiveness of DIP in enhancing siderophore detection. In one study, media supplemented with 100–400 μM DIP yielded high siderophore activity as measured by CAS assay (Nas and Cianciotto, 2017), while no siderophores were detected when iron salts were added to the media, further supporting the central role of iron limitation in regulating production (Nudel et al., 2001).

In this project, bacterial strains were fermented under both iron-deficient conditions (no added iron) and DIP-supplemented conditions. As demonstrated in previous studies, DIP provides a robust and reliable method to induce siderophore biosynthesis (Southwell et al., 2024; Nudel et al., 2001; Nas and Cianciotto, 2017; McHugh et al., 2003), making it a valuable tool for screening unknown isolates. No other changes were made to the media composition or fermentation parameters, and iron accessibility was the sole variable. While other environmental factors may influence siderophore production, they were not investigated here; the aim was to establish whether each strain could produce siderophores in response to iron limitation alone.

2.5 Detection and Quantification of Siderophores

Siderophore detection and characterisation in laboratory studies commonly rely on chemical, colourimetric assays. These tests not only confirm the presence of siderophores but can also provide insight into their chemical class based on specific reactivity.

The most widely used siderophore detection method is the Chrome Azurol S (CAS) assay. This technique is based on an indicator dye complexed with Fe^{3+}, which changes colour from blue to orange-pink when iron is removed by a competing chelator (Payne, 1994). Giving a inverted relationship between colour absorbance and siderophore quantity. The CAS assay is non-specific to siderophore type and detects any compound with sufficient iron affinity. A

simpler qualitative alternative is the ferric chloride test, in which Fe^{3+} reacts with phenolic or hydroxamate siderophores to form coloured complexes (Amsaveni et al., 2016).

To further distinguish between siderophore classes, several class-specific assays have been developed. Catecholate-type siderophores can be detected using the Arnow test, which relies on a two-step reaction with nitrite–molybdate reagent that produces a yellow colour in acidic conditions and turns deep red under alkaline conditions (Ferreira et al., 2019). The Rioux assay offers an additional colourimetric method for detecting catechols (Rioux et al., 1983). Hydroxamate groups can be identified by the Csaky and Atkin assays, both of which involve oxidation of the hydroxamic group followed by colour development (Payne, 1994), as well as the Tetrazolium method (Chowdappa et al., 2020). Carboxylate-type siderophores are less common and are typically detected using the Shenker's assay, which measures complex formation with Fe^{3+} under specific pH conditions (Wang et al., 2022b). All of these tests were employed in this project to detect siderophore activity and to infer the likely class of chelator produced.

3 Methods

This section outlines the experimental procedures used to investigate siderophore production in thermophilic bacterial strains. It includes details on fermentation conditions, glucose metabolism analysis, siderophore detection and classification assays, and the purification of catecholate-type siderophores.

3.1 Bacterial fermentations

Three thermophilic bacterial strains, 7349, 4624, and 623, were fermented for siderophore production. Each strain was incubated in duplicate under three media conditions: iron-rich DRM ("Fe"), iron-depleted DRM with no added iron in the trace element solution ("noFe"), and DRM supplemented with 100μM 2,2'-dipyridyl to further enhance iron limitation ("DIP"). The base DRM formulation followed the recipe described by Mukti et al., including Wolfe's Vitamins and trace elements; full media compositions and modifications are listed in Appendix A.1.

Initial inoculation for the pre-culture was performed by adding thawed bacterial stock to a total 25 mL of Fe-DRM to reactivate the strains. These cultures were grown at 200 rpm in a benchtop shaker incubator (INFORS HT Ecotron) until an optical density (OD_{600}) above 2.5 was reached. Main fermentations were then inoculated at 5% (v/v) into 100 mL of the corresponding DRM variant. All strains were incubated at 200 rpm, with strain 623 maintained at 65°C and strains 7349 and 4624 at 60°C. Inoculum percentages varied slightly depending on the strain and media condition but generally followed an 8% (v/v) inoculum for pre-culture and a 5% inoculum for main fermentation. Full inoculation volumes per strain and condition are detailed in Table 6 in Appendix A.1.

Fermentations were monitored by measuring OD_{600} using a UV/vis spectrophotometer (Biochrom WPA Lightwave II). 2 mL sampling was performed throughout the incubation period, with a larger aliquot of 10 mL taken at stationary phase (usually reached after 9-12 hours). All fermentations were terminated after 24 hours and collected as the final fermentation sample. Culture samples were centrifuged at 3500 g for 30 minutes to pellet cells. The resulting super-

natants were filtered through 0.2 μm membranes and stored at –20 °C until further analysis.

3.1.1 Glucose metabolism by ion chromatography

The rate of glucose metabolism in strain 4624 was determined by ion chromatography. Culture supernatants collected at various time points were diluted prior to analysis: a 200-fold dilution was applied to samples collected between 0–4 hours, and a 50-fold dilution was used for samples from 5–24 hours. All diluted samples were filtered through 0.2 μm membranes into polypropylene vials (DIONEX) and stored at –20 °C until analysis.

Analyses were carried out using a Dionex ICS-5000 ion chromatography system (Thermo Fisher Scientific), equipped with a Dual Pump, an AS-AP Autosampler, and a Detector/Chromatography Module. Separation of monosaccharides was performed on a Dionex CarboPac PA20 analytical column. Mobile phases were prepared according to the protocol by Mukti et al., and consisted of three eluents delivered by separate pumps: Milli-Q water (Solvent A), 20 mM NaOH (Solvent B), and 200 mM NaOH (Solvent C). The chromatographic run proceeded at an isocratic flow rate of 0.5 mL/min with 62.5% Solvent A and 37.5% Solvent B for the first 20 minutes to achieve separation. This was followed by a column-cleaning phase from 20 to 25 minutes using 50% Solvent A and 50% Solvent C. From 25 to 30 minutes, 100% Solvent C was applied to complete the cleaning cycle. The system was then re-equilibrated to 62.5% Solvent A and 37.5% Solvent B before the next sample injection.

Quantification was based on an external calibration curve using glucose standards at concentrations of 5, 10, 20, and 30 mg/L. A representative standard curve is shown in Figure 3 with slope, intercept, and R^2 values reported. All assay runs yielded comparable calibration quality.

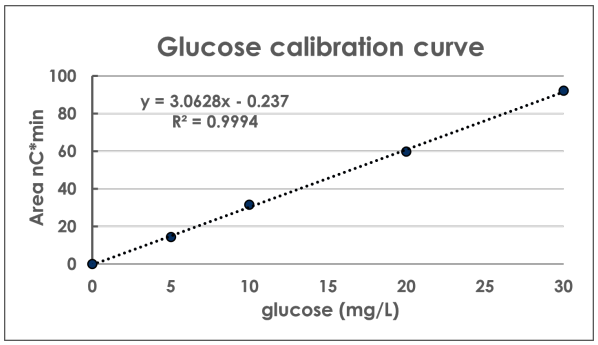

Figure 3: Calibration curve for glucose quantification using ion chromatography. Glucose standards were prepared at 5–30 mg/L. A linear regression yielded the equation y = 3.0628x − 0.237 with a correlation coefficient of $R^2 = 0.9994$. Peak area is expressed in nC × min

3.2 Siderophore detection assays

In the following assays, samples taken at stationary phase as well as the 24 hour mark were analysed. As references and controls, samples of unused bacterial media as well as milli-Q water were run to account for any non-siderophore interactions with the assay.

3.2.1 Chrome Azurol S Liquid Assay

Siderophore activity in fermentation supernatants was quantified using the Chrome Azurol S (CAS) liquid assay, originally developed by Schwyn and Neilands and performed as described by Payne. All samples and corresponding media controls were diluted 1:50 in Milli-Q water prior to analysis to minimise background interference.

The piperazine buffer was prepared by dissolving 4.307 g piperazine in 30 mL water and adjusting the pH to 5.6 with 6.75 mL of 37% HCl. The CAS reaction solution was prepared by dissolving 0.0219 g hexadecyltrimethylammonium bromide (HDTMA) in 50 mL of water. To this, 7.5 mL of 2 mM Chrome Azurol S, and 1.5 mL of 1 mM $FeCl_3 \times 6H_2O$ (prepared in 10 mM HCl) were added, followed by all the piperazine buffer. The solution was made up to 100 mL with water. In the assay, 0.5 mL of the diluted sample was mixed with 0.5 mL of CAS reagent and 10μL of shuttle solution (0.2 M sulfosalicylic acid, accelerates colour development). Absorbance was measured at 630 nm after 5 minutes.

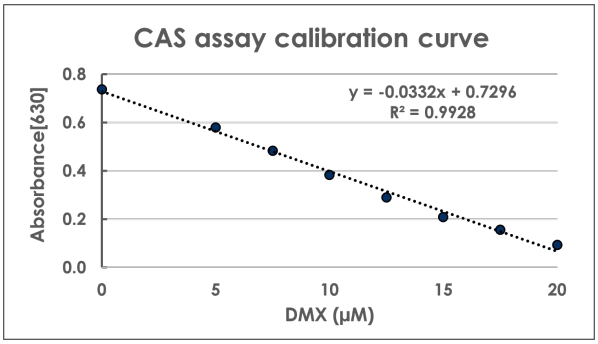

Figure 4: Calibration curve for siderophore detection using CAS liquid assay. DXM standards were prepared at 5–22.5 μM. A linear regression yielded the equation y = - 0.0332x + 0.7296 with a correlation coefficient of $R^2 = 0.9928$. Absorbance was detected at 630 nm.

Quantification was based on a standard curve using desferrioxamine mesylate (DXM) at concentrations of 5, 7.5, 10, 12.5, 15, 17.5, 20, and 22.5 μM (Ferreira et al., 2019). A representative standard curve is shown in Figure 4, with slope, intercept, and R^2 values reported. All assay runs yielded comparable calibration quality.

3.2.2 Ferric Chloride Test

Siderophore presence was further assessed using the ferric chloride assay, performed according to the method of Amsaveni et al.. The assay was conducted in a 96-well microtiter plate by mixing 100 μL of sample with 100 μL of 2% $FeCl_3$ solution. Colour development was measured spectrophotometrically at 500 nm, which was determined to provide the most suitable absorbance values for quantitative comparison.

Quantification was based on a standard curve using desferrioxamine mesylate (DXM) at concentrations of 20, 40, 60, 80, and 100 μM, prepared as described by Liles et al.. A representative standard curve is shown in Figure 5, with slope, intercept, and R^2 values reported. All assay runs yielded comparable calibration quality.

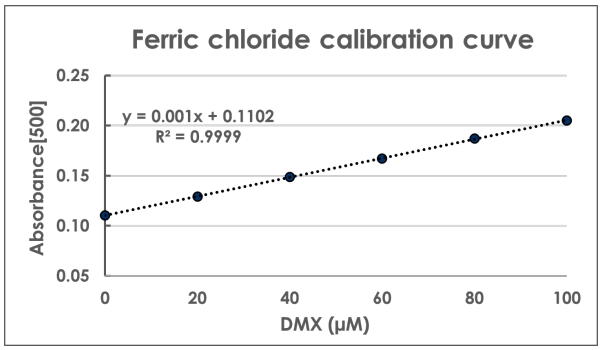

Figure 5: Calibration curve for siderophore detection using the ferric chloride test. DXM standards were prepared at 20–100 μM. A linear regression yielded the equation y = 0.001x + 0.1102 with a correlation coefficient of $R^2 = 0.9999$. Absorbance was detected at 500 nm.

3.2.3 Arnow Assay

Catecholate-type siderophores were detected using the Arnow assay, originally developed by Arnow and performed as described by Ferreira et al.. The assay was carried out in 96-well microtiter plates. To each well, 100 μL of sample was added, followed sequentially by 100 μL of 0.5 M HCl, 100 μL of nitrite–molybdate reagent (prepared by dissolving 10 g sodium nitrite and 10 g sodium molybdate in 100 mL water), and 100 μL of 1 M NaOH. Colour development proceeded for 10 minutes, after which absorbance was measured at 526 nm using a Multiskan GO Microplate Reader.

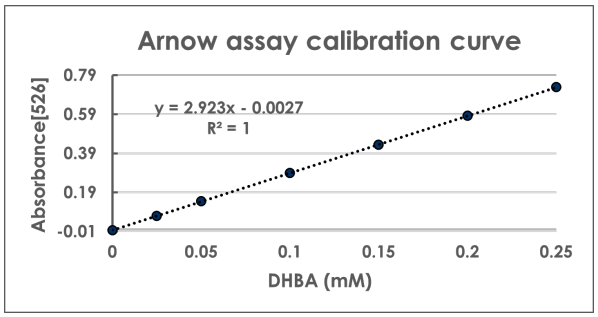

Figure 6: Calibration curve for catecholate detection using the Arnow assay. DHBA standards were prepared at 0.025–0.25 mM. A linear regression yielded the equation y = 2.923x + 0.0027 with a correlation coefficient of $R^2 = 1$. Absorbance was detected at 526 nm.

Quantification was performed using 2,3-dihydroxybenzoic acid (DHBA) as a catecholate standard at concentrations of 0.025, 0.05, 0.1, 0.15, 0.2, and 0.25 mM (Liles et al., 2000). A

representative standard curve is shown in Figure 6, with slope, intercept, and R^2 values reported. All assay runs produced calibration curves of comparable quality, which can be seen summarised in Table 10 in Appendix A.2.3.

3.2.4 Rioux Assay

Catecholate-type siderophores were also detected using the Rioux assay, as originally described by Rioux et al. and performed according to the protocol of Ooi et al.. In each reaction, 0.5 mL of sample was mixed with 1.15 mL of Milli-Q water and 100 μL of concentrated H_2SO_4 in a glass PYREX tube. To this mixture, 0.5 mL of 1% ferric ammonium citrate in 0.09 N H_2SO_4 was added, followed by 200 μL of 2 M ammonium fluoride, 200μL of 1% 1,10-phenanthroline monohydrochloride monohydrate, and 300 μL of 3 M hexamethylenetetramine (HMTA). Tubes were sealed and incubated at 60°C for 1 hour. After cooling to room temperature, absorbance was measured at 510 nm.

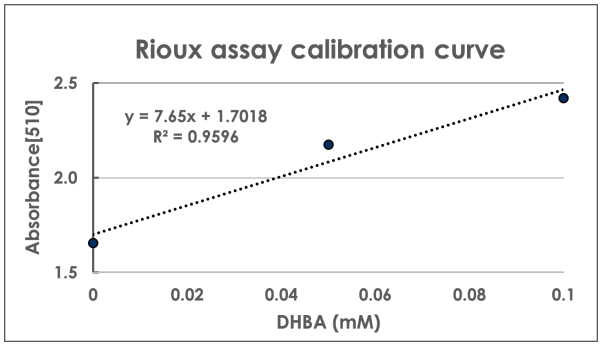

Figure 7: Calibration curve for catecholate detection using the Rioux assay. DHBA standards were prepared at 0–0.1 mM. A linear regression yielded the equation y = 7.65x + 1.7018 with a correlation coefficient of R^2 = 9596. Absorbance was detected at 510 nm.

Quantification was carried out using 2,3-dihydroxybenzoic acid as the standard at concentrations of 0, 0.05 and 0.1 mM (Liles et al., 2000). A representative standard curve is shown in Figure 7, with slope, intercept, and R^2 values reported.

3.2.5 Csaky Assay

Hydroxamate-type siderophores were identified using the Csaky assay, performed as described by Payne. The method detects secondary hydroxamates via acid hydrolysis to nitrite, followed

by diazonium coupling and colourimetric quantification. For each reaction, 0.25 mL of sample was mixed with 0.25 mL of 6 N H_2SO_4 in glass PYREX tubes. Tubes were sealed and hydrolysed at 130°C for 30 minutes, then cooled to room temperature. Next, 0.75 mL of 35% sodium acetate was added, followed by 0.25 mL of 1% sulfanilic acid (prepared in 30% acetic acid). After this, 0.125 mL of iodine solution (1.3% iodine in glacial acetic acid) was added and allowed to react for 5 minutes. Excess iodine was quenched with 0.25 mL of 2% sodium arsenite. Then, 0.25 mL of naphthylamine solution was added, prepared by dissolving 0.3% α-naphthylamine (equivalent to 0.0696 g of n-(1-naphthyl)ethylenediamine dihydrochloride) in 30% acetic acid (Lim and Kim, 1997). Finally, 0.37 mL of Milli-Q water was added to bring the total volume to 2.5 mL. Colour development proceeded for 30 minutes at room temperature. Absorbance was then measured at 526 nm.

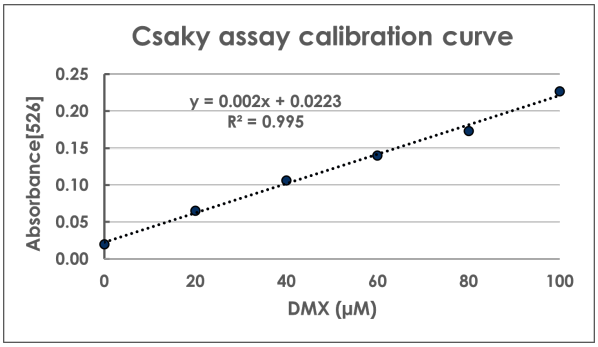

Figure 8: Calibration curve for hydroxamate detection using the Csaky assay. DXM standards were prepared at 20–100 μM. A linear regression yielded the equation y = 0.002x + 0.0223 with a correlation coefficient of R^2 = 995. Absorbance was detected at 526 nm.

Quantification was based on a standard curve generated using desferrioxamine mesylate (DXM) at concentrations of 20, 40, 60, 80, and 100 μM (Liles et al., 2000). A representative standard curve is shown in Figure 8, with slope, intercept, and R^2 values reported.

3.2.6 Atkin Assay

Hydroxamate siderophores were also detected using the Atkin assay, originally developed by Atkin et al.. The assay was carried out in a 96-well microtiter plate by mixing 50 μL of sample with 250 μL of iron perchlorate solution (5 mM iron(III) perchlorate hydrate dissolved in 0.1 M perchloric acid). Colour development proceeded for 5 minutes, after which absorbance was

measured at 480 nm using a Multiskan GO Microplate Reader.

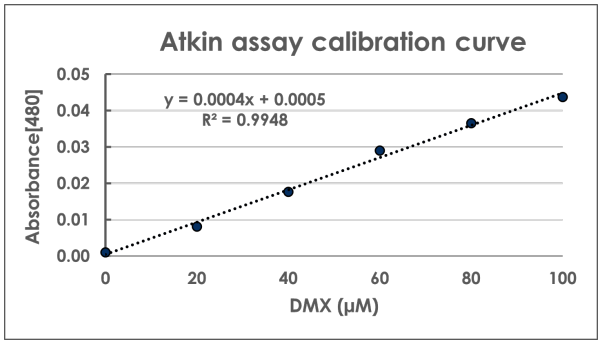

Figure 9: Calibration curve for hydroxamate detection using the Atkin assay. DXM standards were prepared at 20–100 μM. A linear regression yielded the equation y = 0.0004x + 0.0005 with a correlation coefficient of R^2 = 9948. Absorbance was detected at 480 nm.

Quantification was based on a standard curve using desferrioxamine mesylate (DXM) at concentrations of 20, 40, 60, 80, and 100 μM (Liles et al., 2000). A representative standard curve is shown in Figure 9, with slope, intercept, and R^2 values reported.

3.2.7 Tetrazolium test

Hydroxamate siderophores were qualitatively detected using the tetrazolium assay, as described by Chowdappa et al.. In each reaction, one drop of 2 M NaOH was added to 0.5 mL of sample supernatant, followed by the addition of a small scoop of iodonitrotetrazolium chloride. The appearance of a blue colour indicated the presence of hydroxamate-type siderophores. Both 2,3-dihydroxybenzoic acid (0.25, 0.1, and 0.025 mM) and desferrioxamine mesylate (100 μM) was used as a siderophore colour reference. Pictures of standards and media interacting with the assay can be seen in Figure 14 in Appendix A.2.5.

3.2.8 Shenker's Test

Carboxylate-type siderophores were detected using the Shenker assay, performed as described by Wang et al.. The assay was conducted in a 96-well microtiter plate by mixing 100 μL of sample with 100 μL 250 μM $CuSO_4$, followed by 200 μL of acetate buffer adjusted to pH 4. Plates were incubated at room temperature for 30 minutes. Absorbance was then recorded over the range of 200–280 nm using a Multiskan GO Microplate Reader.

3.3 Catecholate Purification

Catecholate-type siderophores from the 4624 fermentation broth were purified using Amberlite™ XAD-2 resin (Merck, Supelco, CAS: 9003-70-7). To achieve a settled bed volume (SBV) of approximately 4 mL, 2.6 g of resin was weighed into a 15 mL Falcon tube. The resin was rinsed twice with 2 bed volumes (BV) of distilled water at 60°C to remove salts and manufacturing residues as recommended by manufacturer (Sigma–Aldrich Corporation, 1997). After decanting the water, 2 BV of methanol (Merck, 99.9% for analysis) was added and the resin was left to swell overnight. Following swelling, the methanol was removed and replaced with 1 BV of 50% methanol:water to ease the polarity transition (Guan et al., 2017; Alevia et al., 2021). This was then decanted, and the resin was rinsed multiple times with Milli-Q water before column packing.

The hydrated resin was gradually packed into a 0.7 × 15 cm Econo-Column (Bio-Rad) until fully settled. The final resin bed height was measured at 10cm, corresponding to an SBV of 3.84 mL. Any remaining resin on the column walls was washed down with 50% methanol:water, followed by additional rinsing with Milli-Q water. The column was connected to a peristaltic pump (ISMATEC) to maintain a constant flow rate during operation.

Filtered fermentation broth (0.45 μm) from the 4624 DIP condition at the 24 hour mark was used as the sample. A total of 26 mL of supernatant was loaded onto the column at a flow rate of approximately 12 mL/h (3 BV/h), and the effluent was collected in 2 mL aliquots. After sample loading, the column was washed with 2 BV of Milli-Q water, followed by elution with 30 mL of pure methanol. All fractions during sample loading, washing, and elution were collected in 2 mL volumes. Upon completion, the column was washed with 50% methanol:water and stored in the same solution.

Evaluation of purification was performed using the Arnow assay for catecholate detection, applied to all collected 2 mL effluent fractions. The assay procedure is described in Section3.2.3.

4 Results

This section presents the outcomes of bacterial fermentations under varying iron conditions, including growth dynamics, siderophore detection using multiple assays, and the initial purification of catecholate compounds from strain 4624. Key findings are supported by statistical analyses and visualised through representative figures and tables.

4.1 Fermentations

Generation times varied across strains and media, but the effects of iron availability were clearly strain-dependent (Figure 10). For strain 4624, generation times remained relatively consistent across all media conditions. The DIP condition showed a slightly shorter mean generation time (0.87 h) compared to Fe (1.43 h) and noFe (1.22 h), the difference may be partially attributable to inoculum variability, as the DIP culture was fermented on a different day.

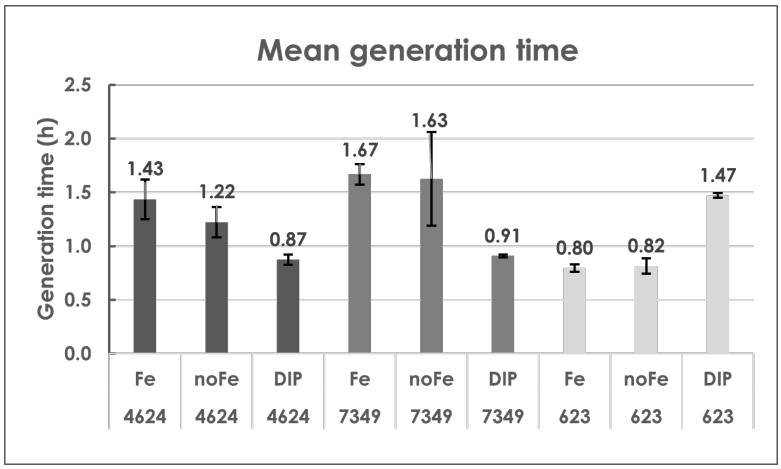

Figure 10: The column chart summarises the mean generation times across the three different strains as well as the three media conditions. The generation times for each of the replicates can be found in Appendix A.2.1 in Table 7.

Strain 7349 showed a more pronounced response. Growth was faster in the DIP condition (0.91 h) compared to Fe (1.67 h) and noFe (1.63 h). As with 4624 this might also be due to inoculum differences as Fe and noFe inoculum were in stationary phase, which might have contributed to the observed lower growth rate than DIP. Despite these limitations, one-way ANOVA indicated a significant difference across media for both 4624 ($p = 0.014$) and 7349 (p

= 0.006), with post hoc interpretation pointing to DIP as the driver of this variation. In contrast, strain 623 showed the opposite trend. All fermentations were conducted simultaneously using the same inoculum, and here, the DIP condition led to a clear increase in generation time (1.47 h), significantly higher than in Fe (0.80 h) or noFe (0.82 h). One-way ANOVA confirmed the significance of this difference (p = 0.002).

Overall, the DIP treatment consistently reduced generation time in the clinical isolates 4624 and 7349, but increased it in the livestock-associated strain 623. Removal of iron alone (noFe) did not significantly affect growth in any strain under these experimental conditions. Note that each condition was tested with only two biological replicates. As such, these p-values should be interpreted as exploratory. Growth curves (Figure 13) and statistical analysis is provided in Appendix A.2.1, full generation time values with the fermentation replicates can be found in Table 7.

4.2 Siderophore determination

Siderophore activity was assessed across all fermentations using a panel of general and class-specific assays. Table 1 summarises the outcome of each test. No strain produced a significant response in the Chrome Azurol S (CAS) assay, and all values remained below the media-corrected baseline (Appendix A.2.2). The ferric chloride assay showed significant differences between media conditions in all strains (two-way ANOVA, $p < 0.005$), but only strain 4624 exhibited a clear trend of increasing siderophore activity with increasing iron limitation (Fe < noFe < DIP).

Strain 4624 consistently tested positive for catecholate siderophores, showing strong media-dependent differences in both the Arnow and Rioux assays (Appendix A.2.3). The Arnow assay in particular showed highly significant elevation in DIP cultures ($p < 0.001$), indicating robust catecholate secretion under iron-chelating conditions. No significant catecholate activity was detected for 7349 or 623. Among the hydroxamate assays, only the Csaky assay returned a significant result (p = 0.044), again in the 4624 DIP sample, though the negative values and high variability limit interpretability (Appendix A.2.4). The Atkin assay showed

Table 1: Summary of siderophore detection assays across all fermentations. Each cell reflects the outcome of a specific assay for a given strain and medium condition. A positive result is denoted by "+", with "++" indicating a strongly positive signal based on statistical significance ($p < 0.05$) or consistent assay response. "+/–" indicates a tentative or ambiguous reaction, while "–" denotes no detectable activity. Full statistical analyses and assay details are provided in Appendix sections A.2.2–A.2.5.

Strain	Media	CAS	$FeCl_3$	Arnow	Rioux	Csaky	Atkin	Tetrazolium	Shenker's
4624	Fe	-	-	-	-	-	-	-	-
4624	noFe	-	+	-	-	-	-	-	-
4624	DIP	-	+	++	+	+	-	-	-
7349	Fe	-	-	-	-	-	-	-	-
7349	noFe	-	-	-	-	-	-	-	-
7349	DIP	-	-	-	-	-	+/-	+	-
623	Fe	-	-	-	-	-	-	-	-
623	noFe	-	-	-	-	-	-	-	-
623	DIP	-	-	-	-	-	-	-	-

no statistically significant trends within any strain, though strain 7349 presented the strongest non-significant indication of hydroxamate presence under DIP. In the Tetrazolium assay, only 7349 DIP samples showed a visually distinct turquoise colour reaction. While the Tetrazolium results are not quantifiable, it may support the tentative hydroxamate signal observed in the Atkin test for strain 7349 (Appendix A.2.5). No evidence of carboxylate-type siderophores was found in any condition based on Shenker's test (Appendix A.2.6).

Together, the results indicate that clinical isolate 4624 is a strong producer of catecholate siderophores under iron-limiting conditions, while 7349 may produce hydroxamates at low levels. Strain 623 showed no conclusive siderophore activity in any assay.

4.3 Catecholate investigation of 4624

To better understand the link between growth, glucose use, and siderophore production in strain 4624, samples from fermentation DIP A were tracked over time (Figure 11).

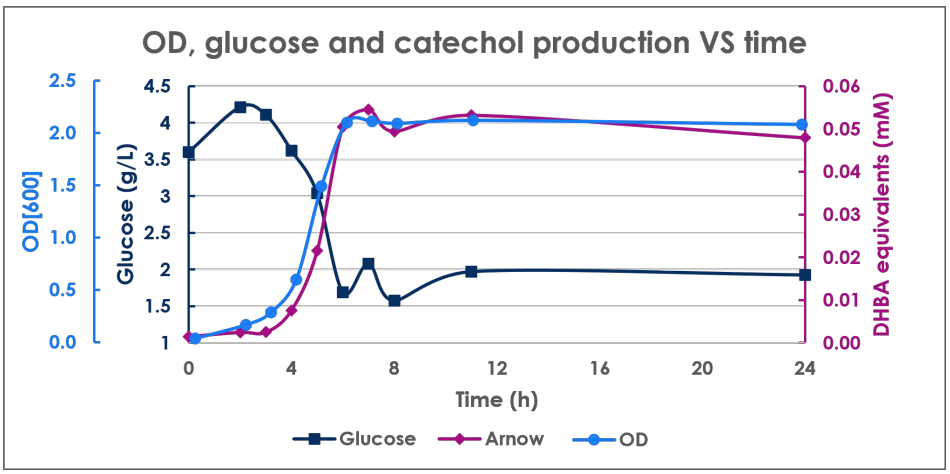

Figure 11: Glucose consumption (Grey), optical density (Blue), and catecholate production in DHBA equivalents (Magenta) are plotted together over time for 4624 fermentation DIP A. Glucose levels declined as OD increased, with catecholate production rising shortly after growth began.

Glucose levels dropped steadily from the start, with the fastest decrease during the exponential growth phase based on OD[600] readings. Catecholate production, measured via the Arnow assay and expressed in DHBA equivalents, began rising just after the onset of exponential growth and closely mirrored the OD curve, albeit with a slight delay. This pattern suggests that catecholate biosynthesis is coupled to the active growth phase rather than being strictly a stationary-phase phenomenon, in agreement with prior reports in *Bacillus megaterium* and *Pseudomonas aeruginosa*, where siderophore production initiates during mid-to-late exponential growth (Santos et al., 2014; Little et al., 2018), and has reached a max yield as the bacteria reaches the stationary phase. The consistent level of catecholates in the 12 hour sample versus the 24 hour sample suggest also some heat stability as the catecholates do no appear to break down after 12 hours of heat exposure at 60°C.

For the other 4624 fermentations the glucose and catecholate measurement results can be found in Appendix A.2.7.

Catecholate purification

To assess the recovery of catecholates from the fermentation broth, the DIP A supernatant from strain 4624 was passed through a column packed with XAD-2 resin, and effluents were

collected in 2 mL aliquots throughout the process. The DHBA equivalents in each fraction were measured using the Arnow assay to evaluate catecholate presence (Figure 12).

The initial sample fractions (1–12) showed a steady increase in catecholate concentration, starting at 0.0274 mM and peaking at 0.0481 mM. This indicates that the resin's binding capacity was reached early, resulting in poor retention and significant product loss during sample loading. Nevertheless, the subsequent water wash (fractions 13–18) showed no detectable catecholate content, suggesting effective retention by the resin and no leakage during the washing step.

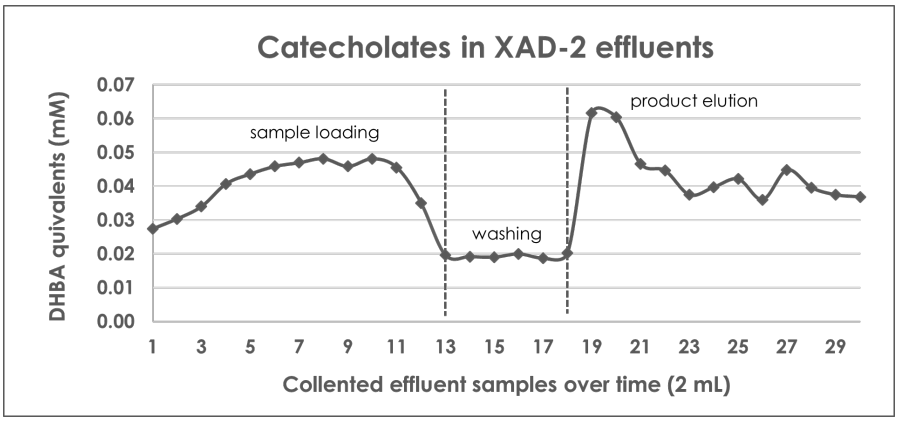

Figure 12: Concentration of catecholates, expressed as DHBA equivalents, in effluents collected during XAD-2 purification of 4624 DIP A fermentation broth. Fractions 1–12 correspond to sample loading, 13–18 to the water wash, and 19–30 to methanol elution.

The methanol elution (fractions 19–30) yielded a strong release of bound catecholates. The first elution fraction peaked at 0.0617 mM DHBA equivalents, thus surpassing the concentrations measured in the sample load and confirming successful capture and partial concentration of the product.

5 Discussion

This project aimed to investigate the potential of thermophilic bacteria isolated from Icelandic hot springs to produce siderophores. The work was motivated by prior genomic analyses conducted by Matís, which used AntiSMASH to identify biosynthetic gene clusters indicative of siderophore production in several thermophilic isolates. While such bioinformatic predictions suggest functional potential, experimental validation is essential to determine whether these pathways are active under iron-limited conditions. The goal of this study was therefore to assess siderophore production across three thermophilic strains using fermentation, chemical detection assays, and preliminary purification approaches, with particular attention to how iron availability affects growth and metabolite release.

5.1 Fermentation Performance and Siderophore Detection

Strain 4624 displayed robust growth across all media conditions, with no apparent consequences in generation time from iron omission or chelation. This suggests that the strain either possesses low iron requirements or compensatory mechanisms to maintain intracellular iron levels. Consistent with the latter, 4624 was the only strain to test significantly positive in a general siderophore assay, the ferric chloride test, and also showed the clearest evidence of specific siderophore types. Both the Arnow and Rioux assays revealed strong catecholate activity in the DIP media, with Arnow results reaching high statistical significance. This pattern supports active catecholate siderophore secretion under iron stress, likely aiding iron acquisition and sustaining growth. Additionally, the Csaky assay indicated possible hydroxamate presence in the DIP sample, though the result was less reliable due to assay instability. Taken together, these findings confirm that strain 4624 not only encodes siderophore genes, but actively expresses them under iron-limited conditions.

Strain 7349 mirrored 4624 in growth trends, maintaining short generation times across all media. Although none of the general or catecholate-specific assays produced a statistically positive result, weak activity was observed in the hydroxamate-specific tests. The Atkin assay suggested a possible increase in hydroxamates in the DIP condition, and the Tetrazolium test

displayed a distinct colour shift only in the DIP samples. While these results fall short of confirmation, they suggest low-level hydroxamate production. This could partly explain the strain's ability to thrive under iron-limited conditions, even in the absence of strong siderophore assay signals. Notably, hydroxamates bind iron with lower affinity than catecholates, and thus, even at comparable concentrations, may produce weaker assay responses. The possibility remains that 7349 synthesises hydroxamate siderophores below current detection thresholds, highlighting the need for more sensitive or targeted approaches to fully evaluate its iron-scavenging potential.

Strain 623, in contrast, exhibited clear sensitivity to iron deprivation. Growth was notably impaired in DIP medium, with extended generation time and reduced final OD, suggesting a stronger dependency on external iron. Crucially, this strain yielded no positive results across any siderophore assay, whether general or class-specific. If siderophore biosynthetic genes are present, as AntiSMASH suggests, they may be poorly expressed under the tested conditions or require alternative triggers beyond simple iron limitation. The combined absence of growth resilience and siderophore signals indicates that strain 623 was unable to mitigate the effects of iron chelation during the fermentation period.

Overall, while all three strains show genomic potential for siderophore biosynthesis, only strain 4624 displayed definitive phenotypic evidence of siderophore expression under iron-limited conditions, particularly of the catecholate type. These results validate the bioinformatic predictions and highlight the importance of linking genome mining with functional screening.

Assay performance and opportunities for fermentation optimisation

While the applied assays enabled preliminary characterisation of siderophore activity, several methodological limitations became apparent. The general tests, CAS and ferric chloride assays, showed notable interaction with the DRM medium, creating limitations determining the results. Most published siderophore studies employ simpler minimal media like MM9, which are less prone to background reactivity and more compatible with colourimetric assays (Southwell et al., 2024; Nudel et al., 2001; Payne, 1994; Murakami et al., 2021). In contrast, the

Arnow assay for catecholates proved both sensitive and robust, delivering reliable catecholate detection across media types. The Rioux assay showed some promise but suffered from high variability between technical replicates, undermining confidence in its reproducibility. Meanwhile, the Tetrazolium test was based on visual scoring of colour change, introducing a level of subjectivity that limits its diagnostic value. Future work should aim to improve assay reliability through inclusion of better controls and by identifying which components of DRM media interfere with iron-reactive dyes.

The use of 2,2'-dipyridyl (DIP) to create iron-limited conditions proved essential for inducing siderophore production. Omitting iron from the media alone was not sufficient to trigger a strong response, indicating that residual iron from inocula or other sources may still support growth. While 100 μM DIP induced detectable siderophore production without compromising viability, this concentration likely represents only a mild level of iron stress. Several studies, including Nas and Cianciotto (2017) and Nakouti and Hobbs (2014), have shown that increasing DIP to 200 μM or more can further elevate siderophore output, up to a point. At very high concentrations (e.g., 400 μM), growth is increasingly impaired, and intracellular iron pools may also become compromised (Nas and Cianciotto, 2017). Exploring a broader DIP gradient in future fermentations could help determine the optimal level for maximal siderophore yield in strain 4624 and clarify whether the hydroxamate trends seen in strain 7349 can be strengthened or confirmed.

Finally, pH control may serve as another lever for optimising siderophore biosynthesis. In acid-producing strains, a drop in pH during fermentation can increase iron solubility, potentially suppressing siderophore gene expression. Maintaining a neutral pH throughout growth may help ensure that iron scarcity is maintained as the dominant stressor, thereby promoting consistent siderophore production. Together, these insights provide a framework for refining both detection methods and cultivation strategies in future investigations.

5.2 Purification of catecholates from 4624 and future isolation perspectives

Given the strong catecholate signal detected in strain 4624, purification of the siderophores was attempted using Amberlite XAD-2 resin. The approach demonstrated proof-of-concept, with partial enrichment of the target compounds and minimal loss during washing. However, the breakthrough curve suggested that the resin's binding capacity was exceeded early in the loading phase, resulting in substantial product loss in the flow-through. Despite this, the methanol elution step yielded a concentrated fraction with a higher catecholate content than the original fermentation broth, confirming that XAD-2 can selectively recover the siderophores.

To improve the recovery and efficiency of XAD-2 purification, several modifications are recommended. First, the resin volume should be increased to match the sample load more appropriately. In this study, approximately 4 mL of resin was used for 26 mL of sample—a roughly 1:6 resin-to-sample ratio, whereas other protocols suggest using a 1:2 ratio or lower to avoid early saturation (Khan et al., 2021). Second, reducing the flow rate or pre-incubating the resin with the sample before packing the column could increase contact time and improve binding efficiency (Supanekar et al., 2013). Lastly, modifying the polarity of the sample by acidifying to pH 2 would protonate ionisable groups on the catecholate scaffold, increasing their affinity for the hydrophobic resin surface (Berner et al., 1991; Khan et al., 2021; Slauenwhite and Wangersky, 1996). This adjustment may also delay breakthrough, allowing a greater proportion of the siderophores to be captured before saturation.

Following successful enrichment with XAD-2, further purification steps can be considered to isolate and identify the main catecholate component. A common next step involves evaporating the methanol eluates to dryness and reconstituting the residues in either water or methanol (Berner et al., 1991; Supanekar et al., 2013). Subsequent fractionation can be achieved by Sephadex LH20 chromatography, which has been used effectively in previous catecholate purification protocols (Khan et al., 2021; De Serrano et al., 2016). Finally, high-resolution separation by reversed-phase C18 HPLC can be used to obtain pure siderophore compounds for structural characterisation. This approach is also compatible with LC–MS analysis, where mobile phases typically consist of Milli-Q water with 0.1 % formic acid and an acetonitrile

gradient, with detection at 260 nm (Hisatomi et al., 2021).

Collectively, these refinements outline a practical route for future studies aiming to isolate thermostable catecholates from thermophilic strains and explore their chemical identities and potential applications.

5.3 Broader implications of the study

This study supports the potential of thermophilic bacteria as a source of siderophores, demonstrating that strain 4624 can produce catecholate-type siderophores when grown at elevated temperatures under iron-limited conditions. While the functional properties of these siderophores remain to be fully characterised, their production at 60°C suggests possible compatibility with high-temperature processes. This may be relevant for industrial or environmental applications where conventional mesophilic systems are less effective or more resource-intensive to maintain. Although the purification was only partially successful, it represents a first step toward isolating and studying these compounds in greater detail. If their structure and stability prove favourable, they may eventually contribute to efforts in areas such as bioremediation, metal recovery, and medical applications.

Overall, the findings help validate earlier genomic predictions and highlight the value of continued exploration of Icelandic thermophiles as a relatively untapped resource in microbial biotechnology.

6 Conclusion

This thesis explored the siderophore-producing potential of thermophilic bacterial strains isolated from Icelandic hot springs. Guided by previous AntiSMASH analyses indicating the presence of siderophore biosynthetic gene clusters, three strains were screened for growth performance and siderophore secretion under varying iron availability. The combination of fermentation profiling, chemical detection assays, and initial purification attempts enabled a functional assessment of this genomic potential.

Of the three strains tested, only strain 4624 exhibited clear phenotypic evidence of siderophore production, particularly of the catecholate type, under iron-limited conditions created by DIP supplementation. The catecholate signal was strong, reproducible, and correlated with active growth, suggesting that these metabolites play a role in iron acquisition during exponential phase. In contrast, strain 7349 showed weak and inconclusive signals, mainly in hydroxamate-specific assays, while strain 623 did not appear to respond to iron limitation at all. These differences highlight the strain-specific nature of siderophore expression and underline the need for both genomic and experimental validation when bioprospecting for novel microbial traits. The partial purification of catecholates from 4624 using XAD-2 resin marked a promising step towards isolating these compounds for structural and functional analysis. Although improvements to the method are necessary, this work lays the foundation for more targeted purification and characterisation efforts.

Ultimately, the findings support the idea that thermophilic bacteria, particularly strain 4624, may serve as viable candidates for the production of siderophores at elevated temperatures. Their ability to function under such conditions opens avenues for application in settings where thermotolerance is advantageous. More broadly, this study contributes to the growing body of evidence that geothermal environments harbour metabolically versatile microbes with potential utility in sustainable and industrial biotechnology.

References

Abraham, C. A., Bradley, K. M., Scully, S. M., Orlygsson, J., Dube, D., and Benner, S. A. (2024). Draft genome of thermoanaerobacter thermohydrosulfuricus strain ak152, a novel thermophilic and anaerobic bacterium isolated from a hot spring in iceland. *Microbiology Resource Announcements*, 13(10):e01175–23.

Ahmed, E. and Holmström, S. J. (2014). Siderophores in environmental research: roles and applications. *Microbial biotechnology*, 7(3):196–208.

Albelda-Berenguer, M., Monachon, M., and Joseph, E. (2019). Siderophores: From natural roles to potential applications. *Advances in applied microbiology*, 106:193–225.

Alevia, M., Rasines, S., Cantero, L., Sancho, M. T., Fernández-Muiño, M. A., and Osés, S. M. (2021). Chemical extraction and gastrointestinal digestion of honey: Influence on its antioxidant, antimicrobial and anti-inflammatory activities. *Foods*, 10(6):1412.

Amsaveni, R., Sureshkumar, M., Aravinth, A., Mary, J. R., and Vivekanandhan, G. (2016). Production of non-ribosomal peptide synthetase (nrps)-dependent siderophore by aeromonas isolates. *Iranian Biomedical Journal*, 20(4):235.

Andrews, S. C., Robinson, A. K., and Rodríguez-Quiñones, F. (2003). Bacterial iron homeostasis. *FEMS microbiology reviews*, 27(2-3):215–237.

Arnow, L. E. (1937). Colorimetric determination of the components of 3,4-dihydroxyphenylalaninetyrosine mixtures. *Journal of Biological Chemistry*, 118(2):531–537.

Atkin, C., Neilands, J., and Phaff, H. (1970). Rhodotorulic acid from species of leucosporidium, rhodosporidium, rhodotorula, sporidiobolus, and sporobolomyces, and a new alanine-containing ferrichrome from cryptococcus melibiosum. *Journal of Bacteriology*, 103(3):722–733.

Baez, A., Sharma, A. K., Bryukhanov, A., Anderson, E. D., Rudack, L., Olivares-Hernández, R., Quan, D., and Shiloach, J. (2022). Iron availability enhances the cellular energetics of aerobic escherichia coli cultures while upregulating anaerobic respiratory chains. *New biotechnology*, 71:11–20.

Bailey, D. C., Bohac, T. J., Shapiro, J. A., Giblin, D. E., Wencewicz, T. A., and Gulick, A. M. (2018). Crystal structure of the siderophore binding protein baub bound to an unusual 2: 1 complex between acinetobactin and ferric iron. *Biochemistry*, 57(48):6653–6661.

Bellenger, J., Wichard, T., Kustka, A., and Kraepiel, A. (2008). Uptake of molybdenum and vanadium by a nitrogen-fixing soil bacterium using siderophores. *Nature Geoscience*, 1(4):243–246.

Berner, I., Greiner, M., Metzger, J., Jung, G., and Winkelmann, G. (1991). Identification of enterobactin and linear dihydroxybenzoylserine compounds by hplc and ion spray mass spectrometry (lc/ms and ms/ms). *Biology of metals*, 4:113–118.

Bjornsdottir, S. H., Petursdottir, S. K., Hreggvidsson, G. O., Skirnisdottir, S., Hjorleifsdottir, S., Arnfinnsson, J., and Kristjansson, J. K. (2009). Thermus islandicus sp. nov., a mixotrophic sulfur-oxidizing bacterium isolated from the torfajokull geothermal area. *International journal of systematic and evolutionary microbiology*, 59(12):2962–2966.

Bleuel, C., Große, C., Taudte, N., Scherer, J., Wesenberg, D., Krauß, G. J., Nies, D. H., and Grass, G. (2005). Tolc is involved in enterobactin efflux across the outer membrane of escherichia coli. *Journal of bacteriology*, 187(19):6701–6707.

Braud, A., Hoegy, F., Jezequel, K., Lebeau, T., and Schalk, I. J. (2009). New insights into the metal specificity of the pseudomonas aeruginosa pyoverdine–iron uptake pathway. *Environmental microbiology*, 11(5):1079–1091.

Burkhardt, C., Baruth, L., Meyer-Heydecke, N., Klippel, B., Margaryan, A., Paloyan, A., Panosyan, H. H., and Antranikian, G. (2024). Mining thermophiles for biotechnologically relevant enzymes: evaluating the potential of european and caucasian hot springs. *Extremophiles*, 28(1):5.

Butler, A. and Theisen, R. M. (2010). Iron (iii)–siderophore coordination chemistry: Reactivity of marine siderophores. *Coordination chemistry reviews*, 254(3-4):288–296.

Cain, T. J. and Smith, A. T. (2021). Ferric iron reductases and their contribution to unicellular ferrous iron uptake. *Journal of inorganic biochemistry*, 218:111407.

Choi, S., Kronstad, J. W., and Jung, W. H. (2024). Siderophore biosynthesis and transport systems in model and pathogenic fungi. *Journal of microbiology and biotechnology*, 34(8):1551.

Chowdappa, S., Jagannath, S., Konappa, N., Udayashankar, A. C., and Jogaiah, S. (2020). Detection and characterization of antibacterial siderophores secreted by endophytic fungi from cymbidium aloifolium. *Biomolecules*, 10(10):1412.

Crowther, T. W., Rappuoli, R., Corinaldesi, C., Danovaro, R., Donohue, T. J., Huisman, J., Stein, L. Y., Timmis, J. K., Timmis, K., Anderson, M. Z., et al. (2024). Scientists' call to action: Microbes, planetary health, and the sustainable development goals. *Cell*, 187(19):5195–5216.

De Serrano, L. O., Camper, A. K., and Richards, A. M. (2016). An overview of siderophores for iron acquisition in microorganisms living in the extreme. *Biometals*, 29:551–571.

Deb, C. R. and Tatung, M. (2024). Siderophore producing bacteria as biocontrol agent against phytopathogens for a better environment: A review. *South African Journal of Botany*, 165:153–162.

Del Hierro, A. G., Moreno-Cid, J. A., and Casey, E. (2024). Continuous biomanufacturing for sustainable bioeconomy applications. *EFB Bioeconomy Journal*, 4:100071.

Fandi, K., Massadeh, M., and Tawaha, A. (2024). Diversity of bioactive metabolites produced by thermophilic bacillus strains isolated from jordanian hot springs. *Jordan Journal of Biological Sciences*, 17(2).

Featherstone, S. (2015). *A complete course in canning and related processes: Volume 3 Processing Procedures for Canned Food Products*. Woodhead Publishing.

Ferreira, C. M., Vilas-Boas, Â., Sousa, C. A., Soares, H. M., and Soares, E. V. (2019). Comparison of five bacterial strains producing siderophores with ability to chelate iron under alkaline conditions. *AMB Express*, 9(1):78.

Gallo, G., Imbimbo, P., and Aulitto, M. (2024). The undeniable potential of thermophiles in industrial processes. *International Journal of Molecular Sciences*, 25(14):7685.

Gao, H. and Span, I. (2025). The diversity and applications of microbial iron metabolism and iron-containing proteins. *Communications Biology*, 8(1):177.

Gräff, Á. T. and Barry, S. M. (2024). Siderophores as tools and treatments. *npj Antimicrobials and Resistance*, 2(1):1–17.

Gu, S., Shao, J., He, R., Xiong, G., Qu, Z., Shao, Y., Yu, L., Zhang, D., Wang, F., Xu, R., et al. (2025). Forging the iron-net: Towards a quantitative understanding of microbial communities via siderophore-mediated interactions. *Quantitative Biology*, 13(2):e84.

Guan, Y., Wang, X., Wong, M., Sun, G., An, T., Guo, J., and Zhang, G. (2017). Evaluation of genotoxic and mutagenic activity of organic extracts from drinking water sources. *PloS one*, 12(1):e0170454.

Guo, L., Brugger, K., Liu, C., Shah, S. A., Zheng, H., Zhu, Y., Wang, S., Lillestøl, R. K., Chen, L., Frank, J., et al. (2011). Genome analyses of icelandic strains of sulfolobus islandicus, model organisms for genetic and virus-host interaction studies. *Journal of bacteriology*, 193(7):1672–1680.

Haki, G. and Rakshit, S. (2003). Developments in industrially important thermostable enzymes: a review. *Bioresource technology*, 89(1):17–34.

Hider, R. C. and Kong, X. (2010). Chemistry and biology of siderophores. *Natural product reports*, 27(5):637–657.

Himpsl, S. D. and Mobley, H. L. T. (2019). *Siderophore Detection Using Chrome Azurol S and Cross-Feeding Assays*, pages 97–108. Springer New York, New York, NY.

Hisatomi, A., Shiwa, Y., Fujita, N., Koshino, H., and Tanaka, N. (2021). Idification and structural characterisation of a catecholate-type siderophore produced by stenotrophomonas maltophilia k279a. *Microbiology*, 167(7):001071.

Hofmann, M., Heine, T., Malik, L., Hofmann, S., Joffroy, K., Senges, C. H. R., Bandow, J. E., and Tischler, D. (2021). Screening for microbial metal-chelating siderophores for the removal of metal ions from solutions. *Microorganisms*, 9(1):111.

Hu, W. and Zheng, H. (2021). Cryo-em reveals unique structural features of the fhucdb escherichia coli ferrichrome importer. *Communications Biology*, 4(1):1383.

Ito, T. and Neilands, J. (1958). Products of "low-iron fermentation" with bacillus subilis: isolation, characterization and synthesis of 2, 3-dihydroxybenzoylglycine1, 2. *Journal of the American Chemical Society*, 80(17):4645–4647.

Izumi, M., Tomita, H., Miyazaki, K., Otsuka, R., and Honda, K. (2025). Biosynthetic characterization of bacillibactin in thermophilic bacillaceae and its potential for in vitro mutational synthesis. *ChemBioChem*, 26(5):e202400836.

Jenner, M., Hai, Y., Nguyen, H. H., Passmore, M., Skyrud, W., Kim, J., Garg, N. K., Zhang, W., Ogorzalek Loo, R. R., and Tang, Y. (2023). Elucidating the molecular programming of a nonlinear non-ribosomal peptide synthetase responsible for fungal siderophore biosynthesis. *Nature Communications*, 14(1):2832.

Keseler, I. M., Mackie, A., Santos-Zavaleta, A., Billington, R., Bonavides-Martínez, C., Caspi, R., Fulcher, C., Gama-Castro, S., Kothari, A., Krummenacker, M., et al. (2017). The ecocyc database: reflecting new knowledge about escherichia coli k-12. *Nucleic acids research*, 45(D1):D543–D550.

Khan, A., Singh, P., Kumar, R., Das, S., Singh, R. K., Mina, U., Agrawal, G. K., Rakwal, R., Sarkar, A., and Srivastava, A. (2021). Antifungal activity of siderophore isolated from escherichia coli against aspergillus nidulans via iron-mediated oxidative stress. *Frontiers in Microbiology*, 12:729032.

Konetschny-Rapp, S., Jung, G., Meiwes, J., and Zähner, H. (1990). Staphyloferrin a: a structurally new siderophore from staphylococci. *European Journal of Biochemistry*, 191(1):65–74.

Kumar, A., Chakravorty, S., Yang, T., Russo, T. A., Newton, S. M., and Klebba, P. E. (2024). Siderophore-mediated iron acquisition by klebsiella pneumoniae. *Journal of Bacteriology*, 206(5):e00024–24.

Kümpel, C., Grosser, M., Tanabe, T. S., and Dahl, C. (2024). Fe/s proteins in microbial sulfur oxidation. *Biochimica et Biophysica Acta (BBA)-Molecular Cell Research*, page 119732.

LeBlanc, A. R. and Wuest, W. M. (2024). Siderophores: A case study in translational chemical biology. *Biochemistry*, 63(15):1877–1891.

Liles, M. R., Scheel, T. A., and Cianciotto, N. P. (2000). Discovery of a nonclassical siderophore, legiobactin, produced by strains of legionella pneumophila. *Journal of bacteriology*, 182(3):749–757.

Lim, H.-S. and Kim, S.-D. (1997). Role of siderophores in biocontrol of fusarium solani and enhanced growth response of bean by pseudomonas fluorescens gl20. *Journal of Microbiology and Biotechnology*, 7(1):13–20.

Little, A. S., Okkotsu, Y., Reinhart, A. A., Damron, F. H., Barbier, M., Barrett, B., Oglesby-Sherrouse, A. G., Goldberg, J. B., Cody, W. L., Schurr, M. J., et al. (2018). Pseudomonas aeruginosa algr phosphorylation status differentially regulates pyocyanin and pyoverdine production. *MBio*, 9(1):10–1128.

Mamo, G., Gashe, B., and Gessesse, A. (1999). A highly thermostable amylase from a newly isolated thermophilic bacillus sp. wn11. *Journal of Applied Microbiology*, 86(4):557–560.

Manck, L. E., Park, J., Tully, B. J., Poire, A. M., Bundy, R. M., Dupont, C. L., and Barbeau, K. A. (2022). Petrobactin, a siderophore produced by alteromonas, mediates community iron acquisition in the global ocean. *The ISME Journal*, 16(2):358–369.

McHugh, J. P., Rodríguez-Quiñones, F., Abdul-Tehrani, H., Svistunenko, D. A., Poole, R. K., Cooper, C. E., and Andrews, S. C. (2003). Global iron-dependent gene regulation in escherichia coli: a new mechanism for iron homeostasis. *Journal of Biological Chemistry*, 278(32):29478–29486.

Medema, M. H., Blin, K., Cimermancic, P., De Jager, V., Zakrzewski, P., Fischbach, M. A., Weber, T., Takano, E., and Breitling, R. (2011). antismash: rapid identification, annotation and analysis of secondary metabolite biosynthesis gene clusters in bacterial and fungal genome sequences. *Nucleic acids research*, 39(suppl_2):W339–W346.

Mehta, R., Singhal, P., Singh, H., Damle, D., and Sharma, A. K. (2016). Insight into thermophiles and their wide-spectrum applications. *3 Biotech*, 6:1–9.

Miethke, M. and Marahiel, M. A. (2007). Siderophore-based iron acquisition and pathogen control. *Microbiology and molecular biology reviews*, 71(3):413–451.

Mukti, I. J., Sardari, R. R., Kristjansdottir, T., Hreggvidsson, G. O., and Karlsson, E. N. (2022). Medium development and production of carotenoids and exopolysaccharides by the extremophile rhodothermus marinus dsm16675 in glucose-based defined media. *Microbial Cell Factories*, 21(1):220.

Murakami, C., Tanaka, A. R., Sato, Y., Kimura, Y., and Morimoto, K. (2021). Easy detection of siderophore production in diluted growth media using an improved cas reagent. *Journal of Microbiological Methods*, 189:106310.

Murray, C. J., Ikuta, K. S., Sharara, F., Swetschinski, L., Aguilar, G. R., Gray, A., Han, C., Bisignano, C., Rao, P., Wool, E., et al. (2022). Global burden of bacterial antimicrobial resistance in 2019: a systematic analysis. *The lancet*, 399(10325):629–655.

Nair, A., Juwarkar, A. A., and Singh, S. K. (2007). Production and characterization of siderophores and its application in arsenic removal from contaminated soil. *Water, Air, and Soil Pollution*, 180:199–212.

Nakouti, I. and Hobbs, G. (2014). Incorporation of l-lysine and 2, 2'-dipyridyl in the growth media promotes desferrioxamine e production by an actinobacterium. *World Journal of Microbiology and Biotechnology*, 30:331–334.

Nas, M. Y. and Cianciotto, N. P. (2017). Stenotrophomonas maltophilia produces an entc-dependent catecholate siderophore that is distinct from enterobactin. *Microbiology*, 163(11):1590–1603.

Nudel, C., Gonzalez, R., Castañeda, N., Mahler, G., and Actis, L. A. (2001). Influence of iron on growth, production of sidero bore compounds, membrane proteins, and lipase activity in acinetobacter calcoaceticus bd 413. *Microbiological research*, 155(4):263–269.

Ooi, Y. S., Nor, N. M. M., Furusawa, G., Tharek, M., and Ghazali, A. H. (2022). Application of bacterial endophytes to control bacterial leaf blight disease and promote rice growth. *The Plant Pathology Journal*, 38(5):490.

Panda, A. K., Bisht, S. S., De Mandal, S., and Kumar, N. S. (2019). Microbial diversity of thermophiles through the lens of next generation sequencing. In *Microbial diversity in the genomic era*, pages 217–226. Elsevier.

Pandey, K., Pandey, M., Kumar, V., Aggarwal, U., and Singhal, B. (2024). Bioprocessing 4.0 in biomanufacturing: paving the way for sustainable bioeconomy. *Systems Microbiology and Biomanufacturing*, 4(2):407–424.

Pattanakittivorakul, S., Kumakiri, I., Nutaratat, P., Hara, M., Yokota, M., Murata, M., Kosaka, T., Thanonkeo, P., Limtong, S., and Yamada, M. (2024). High-temperature fermentation and its downstream processes for compact-scale bioethanol production. *Fuels*, 5(4):857–867.

Payne, S. M. (1994). [25] detection, isolation, and characterization of siderophores. *Methods in enzymology*, 235:329–344.

Podar, P. T., Yang, Z., Björnsdóttir, S. H., and Podar, M. (2020). Comparative analysis of microbial diversity across temperature gradients in hot springs from yellowstone and iceland. *Frontiers in Microbiology*, 11:1625.

Pushparaj, K., Meyyazhagan, A., Bhotla, H. K., Arumugam, V. A., Pappuswamy, M., Vadivalagan, C., Hakeem, K. R., Balasubramanian, B., Liu, W., and Khaneghah, A. M. (2023). The crux of bioactive metabolites in endophytic and thermophilic fungi and their proximal prospects in biotechnological and industrial domains. *Toxicon*, 223:107007.

Raymond, K. N., Dertz, E. A., and Kim, S. S. (2003). Enterobactin: an archetype for microbial iron transport. *Proceedings of the national academy of sciences*, 100(7):3584–3588.

Rioux, C., Jordan, D., and Rattray, J. B. (1983). Colorimetric determination of catechol siderophores in microbial cultures. *Analytical Biochemistry*, 133(1):163–169.

Rocha, B. M., Pinto, E., Sousa, E., and Resende, D. I. (2025). Targeting siderophore biosynthesis to thwart microbial growth. *International Journal of Molecular Sciences*, 26(8):3611.

Santos, S., Neto, I. F., Machado, M. D., Soares, H. M., and Soares, E. V. (2014). Siderophore

production by bacillus megaterium: effect of growth phase and cultural conditions. *Applied biochemistry and biotechnology*, 172:549–560.

Schaible, U. E. and Kaufmann, S. H. (2004). Iron and microbial infection. *Nature Reviews Microbiology*, 2(12):946–953.

Schwyn, B. and Neilands, J. (1987). Universal chemical assay for the detection and determination of siderophores. *Analytical biochemistry*, 160(1):47–56.

Sexton, D. J., Glover, R. C., Loper, J. E., and Schuster, M. (2017). Pseudomonas protegens pf-5 favours self-produced siderophore over free-loading in interspecies competition for iron. *Environmental Microbiology*, 19(9):3514–3525.

Shaw, J.-F., Lin, F.-P., Chen, S.-C., and Chen, H.-C. (1995). Purification and properties of an extracellular a-amylase from thermus sp. *Botanical Bulletin of Academia Sinica*, 36.

Shin, S. H., Lim, Y., Lee, S. E., Yang, N. W., and Rhee, J. H. (2001). Cas agar diffusion assay for the measurement of siderophores in biological fluids. *Journal of microbiological methods*, 44(1):89–95.

Sigma–Aldrich Corporation (1997). Amberlite® xad-2: Technical data sheet. *Product Information Bulletin*. Catalog No. XAD-2, 4 pp.

Silale, A. and van den Berg, B. (2023). Tonb-dependent transport across the bacterial outer membrane. *Annual review of microbiology*, 77(1):67–88.

Sitara, A., Hocq, R., Horvath, J., and Pflügl, S. (2024). Industrial biotechnology goes thermophilic: Thermoanaerobes as promising hosts in the circular carbon economy. *Bioresource Technology*, page 131164.

Skaar, E. P. (2010). The battle for iron between bacterial pathogens and their vertebrate hosts. *PLoS pathogens*, 6(8):e1000949.

Slauenwhite, D. E. and Wangersky, P. J. (1996). Extraction of marine organic matter on xad-2: effect of sample acidification and development of an in situ pre-acidification technique. *Marine chemistry*, 54(1-2):107–117.

Southwell, J. W., Wilson, K. S., Thomas, G. H., and Duhme-Klair, A.-K. (2024). Enhancement of growth media for extreme iron limitation in escherichia coli. *Access microbiology*, 6(6):000735–v4.

Supanekar, S., Sorty, A., and Raut, A. (2013). Study of catechol siderophore from a newly isolated azotobacter sp. sup-iii for its antimicrobial property. *Journal of microbiology, biotechnology and food sciences*, 3(3):270–273.

Tsylents, U., Burmistrz, M., Wojciechowska, M., Stępień, J., Maj, P., and Trylska, J. (2024). Iron uptake pathway of escherichia coli as an entry route for peptide nucleic acids conjugated with a siderophore mimic. *Frontiers in Microbiology*, 15:1331021.

Vraspir, J. M. and Butler, A. (2009). Chemistry of marine ligands and siderophores. *Annual review of marine science*, 1(1):43–63.

Wang, M., Zhang, Y., Lv, L., Kong, D., and Niu, G. (2022a). Biosynthesis and chemical synthesis of albomycin nucleoside antibiotics. *Antibiotics*, 11(4):438.

Wang, Y., Huang, W., Li, Y., Yu, F., and Penttinen, P. (2022b). Isolation, characterization, and evaluation of a high-siderophore-yielding bacterium from heavy metal–contaminated soil. *Environmental Science and Pollution Research*, 29:3888–3899.

Warchold, A. and Pradhan, P. (2025). Bioeconomy and sustainable development goals: How do their interactions matter? *Geography and Sustainability*, 6(3):100293.

Winkelmann, G. (1991). *CRC handbook of microbial iron chelates*. CRC Press Boca Raton.

Yi, S., Li, F., Wu, C., Wei, M., Tian, J., and Ge, F. (2022). Synergistic leaching of heavy metal-polycyclic aromatic hydrocarbon in co-contaminated soil by hydroxamate siderophore: role of cation-π and chelation. *Journal of Hazardous Materials*, 424:127514.

Zheng, S., Shao, M., Wang, W., and Chen, G.-Q. (2025). Next-generation biotechnology inspired by extremes: The potential of extremophile organisms for synthetic biology and for more efficient and sustainable biotechnology. *EMBO reports*, 26(5):1191–1195.

A Appendix

A.1 Media composition

The media used to grow strain 7349, 4624 and 623 is referred to as "DRM" (Defined *Rhodothermus* Medium), and was prepared as described by (Mukti et al., 2022). The media stock solutions in Table 2 can be found in the article supplementary information under table S3. All stock solutions were prepared in acid treated glass bottles and autoclaved for 20 minutes at 121°C, except Solution E which was sterilised with a 0.2 μm bottle top vacuum filter. Solution A and C were adjusted to pH 7.2 with NaOH ahead of sterilisation.

Table 2: The table shows an overview of the DRM stock solutions and their composition. Milli-Q water was used as media solvent. All stock solutions were stored at 4°C between each use.

Stock	**Components**	**Concentration (g/L)**
Solution A	Nitriloacetic acid	10
	$MgCl_2 \times 6H_2O$	10
	NaCl	50
Solution B	$CaSO_4 \times 2H_2O$	2
Solution C	KH_2PO_4	27.22
	Na_2HPO_4	28.39
Solution D	NH_4Cl	53.49
Solution E	Glucose	100

Table 3 shows the composition of the Wolfe's trace elements and Vitamin's solution used in the DRM media (Mukti et al., 2022). The trace elements solution was adjusted to pH 7 with 2 M KOH to allow dissolution of all components. Both solutions were sterilised by autoclaving. The 2,2 dipyridil (DIP) stock solution was prepared by making a 20 mM solution and sterilising it with a 0.2 μm bottle top vacuum filter. The final concentration of DIP in the media would be 100 μM using the media preparation table below.

Table 3: The table shows the composition of the Wolfe's Trace element and Vitamin solutions used in the DRM media. * - in the DRM media without iron a modified trace elements solution was made in which $FeSO_4 \times 7H_2O$ was omitted.

Trace element	Amount (g/L)	Vitamin	Amount (mg/L)
Nitrilotriacetic acid	1.5	Thioctic acid	5.0
$MgSO_4 \times 7H_2O$	3.0	Folic acid	2.0
NaCl	1.0	Riboflavin	5.0
$FeSO_4 \times 7H_2O$*	0.1	Thiamine hydrochloride	5.0
$MnSO_4 \times H_2O$	0.5	Nicotinic acid	5.0
$CoCl_2 \times 6H_2O$	0.1	Biotin	2.0
$CaCl_2$	0.1	Ca-pantothenate	5.0
$ZnSO_4 \times 7H_2O$	0.1	Cobalamine	0.1
$CuSO_4 \times 5H_2O$	0.01	p-Aminobenzoic acid	5.0
$AlK(SO_4)_2 \times 12H_2O$	0.01	Pyridoxine hydrochloride	10.0
$Na_2MoO_4 \times 2H_2O$	0.01		
H_3BO_3	0.01		

Table 4 and 5 was used to mix the necessary amounts of the three different DRM media. The first mentioned table was used for iron and iron-free conditions in which the trace elements without iron was used in the latter. The second table was used when mixing the DRM media containing 100 μM DIP. The DIP media also used the trace elements solution which omitted the addition of iron. All media was mixed fresh right before bacterial inoculation and pH was adjusted to 7.2 using sterile 6 M NaOH.

Table 4: The table lists all the components of the DRM media for the iron and iron free fermentations, and at which amounts they were mixed to achieve the desired amount. * - in the DRM media without iron a modified trace elements solution was made in which $FeSO_4 \times 7H_2O$ was omitted.

	Amount added (mL)					
Solution A	200	100	80	40	20	10
Solution B	200	100	80	40	20	10
Solution C	50	25	20	10	5	2.5
Solution D	10	5	4	2	1	0.5
Solution E	50	25	20	10	5	2.5
Vitamins	5	2.5	2	1	0.5	0.25
Trace elements*	5	2.5	2	1	0.5	0.25
Water	480	240	192	96	48	24
Total media	1000	500	400	200	100	50

Table 5: The table lists all the components of the DRM media for the iron free fermentations containing DIP, and at which amounts they were mixed to achieve the desired amount.

	Amount added (mL)					
Solution A	200	100	80	40	20	10
Solution B	200	100	80	40	20	10
Solution C	50	25	20	10	5	2.5
Solution D	10	5	4	2	1	0.5
Solution E	50	25	20	10	5	2.5
Vitamins	5	2.5	2	1	0.5	0.25
Trace elements - noFe	5	2.5	2	1	0.5	0.25
DIP	5	2.5	2	1	0.5	0.25
Water	475	237.5	190	95	47.5	23.75
Total Media	1000	500	400	200	100	50

The table below lists all the fermentation conditions and the percentage of inoculum in the pre-culture as well as the fermentations. The pre-cultures were prepared in 25 mL while all fermentations were performed in 100 mL cultures. Each of the fermentations listed were performed in duplicates named "A" and "B". At the point where stationary phase was deemed reached a larger aliquot of sample was taken (10 mL).

Table 6: An overview of the percentage of all the pre-culture inoculums as well as all the fermentations performed. The hour at which stationary phase was reached in the fermentations is also mentioned

Strain	Media	Pre-culture inoculum (%)	Fermentation inoculum (%)	Stationary phase (h)
4624	Fe	16	5	9
4624	noFe	16	5	9
4624	DIP	8	5	11
7349	Fe	8	5	12
7349	noFe	8	5	12
7349	DIP	5	5	11
623	Fe	8	5	9
623	noFe	8	5	9
623	DIP	8	5	9

A.2 Supplementary results data

In this section any data to support the results can be found.

A.2.1 Fermentation

In Figure 13 the collective growth curves from all the fermentation can be found. The graphs are supplemented with the data in Table 7 containing the generation times for all the fermentations. Generations times for all the fermentation was obtained by calculating the natural logarithm of the exponential phase of bacterial growth. The slope of the new plotted values were known as the specific growth rate μ, from which the generation times was calculated.

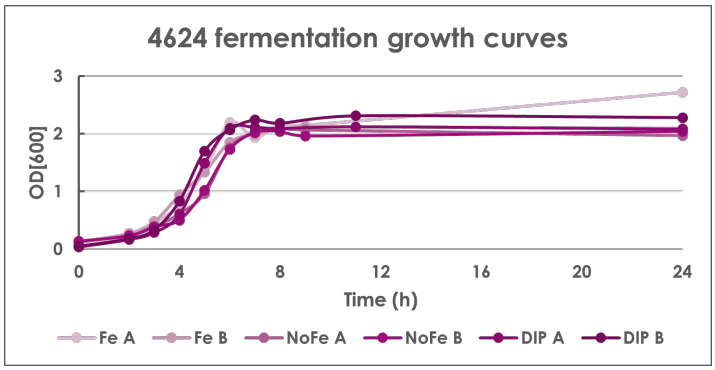

(a) All fermentation growth curves for the strain 4624.

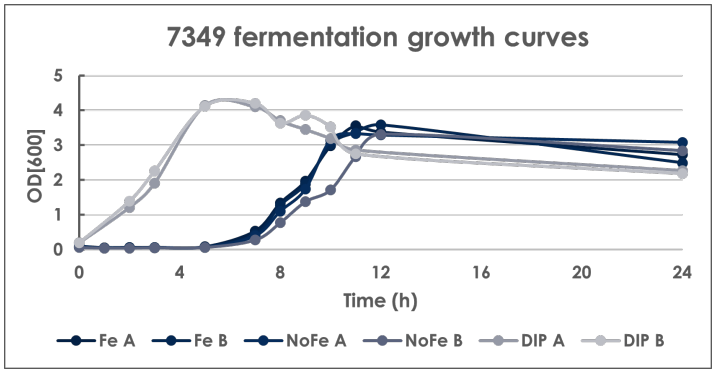

(b) All fermentation growth curves for the strain 7349.

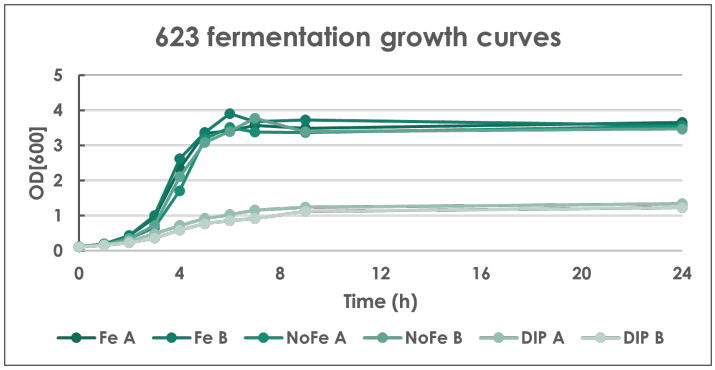

(c) All fermentation growth curves for the strain 623.

Figure 13: The three figures depict the bacterial growth in the three bacterial strains over the course of 24 hours. The growth was measured in optical density at 600 nm.

Two-way ANOVA revealed that both the bacterial strain and the type of medium had a statistically significant effect on generation time ($p = 0.0007$ and $p = 0.0003$, respectively), with a significant interaction between the two factors ($p = 0.00002$). This indicates that the response to iron availability varies depending on the strain.

Table 7: The table shows all the generation times for each performed fermentation as well as the mean and standard deviation between the two replicate fermentations performed for each condition. The generation time is the time it took for the bacterial population to double (h).

Strain	Media	Replicate		Mean generation	Standard
		A	B	time	deviation
4624	Fe	1.303	1.565	1.434	0.185
4624	noFe	1.321	1.121	1.221	0.141
4624	DIP	0.840	0.908	0.874	0.048
7349	Fe	1.735	1.600	1.668	0.095
7349	noFe	1.318	1.934	1.626	0.436
7349	DIP	0.917	0.899	0.908	0.013
623	Fe	0.821	0.771	0.796	0.035
623	noFe	0.866	0.766	0.816	0.071
623	DIP	1.457	1.485	1.471	0.020

Strain-specific one-way ANOVA tests further supported this conclusion. For strain 4624, generation time differed significantly across media ($p = 0.014$), with growth being fastest in the DIP condition. Fe and noFe media showed no distinguishable difference at the given number of fermentation repeats. Strain 7349 followed a similar pattern ($p = 0.006$), with significantly shorter generation times in the DIP condition, while Fe and noFe remained statistically similar. In contrast, strain 623 exhibited an opposite trend ($p = 0.002$): growth was significantly slower in DIP medium, whereas noFe and Fe conditions were statistically indistinguishable.

A.2.2 CAS and Ferric Chloride test

Chrome Azurol S (CAS) assay results indicated no detectable siderophore activity in any strain–media combination. Following correction with media samples, all DXM equivalent values became slightly negative, suggesting the colour change seen in the raw measurements was largely attributable to media interactions with the reagent rather than siderophore binding.

Two-way ANOVA found no significant effect of strain ($p = 0.37$), medium ($p = 0.26$), or their interaction ($p = 0.54$). Likewise, one-way ANOVA tests within each strain yielded no signifi-

Table 8: The table shows the results from the CAS assay performed on all 24 hour samples. The values are shown in equivalents of desferrioxamine mesylate (DXM), calculated using the calibration curve in Figure 4.

		DXM equivalents			
Strain	Fermentation	Rep A	Rep B	Mean	St.dev
7349	Fe	-0.238	-0.244	-0.241	0.003
7349	noFe	-0.240	-0.251	-0.245	0.005
7349	DIP	-0.250	-0.241	-0.245	0.004
4624	Fe	-0.248	-0.243	-0.246	0.002
4624	noFe	-0.247	-0.243	-0.245	0.002
4624	DIP	-0.250	-0.249	-0.250	0.000
623	Fe	-0.249	-0.246	-0.248	0.002
623	noFe	-0.262	-0.253	-0.257	0.004
623	DIP	-0.256	-0.251	-0.253	0.003

cant differences across media (4624: $p = 0.76$; 7349: $p = 0.55$; 623: $p = 0.12$). These results collectively confirm that the CAS assay did not reveal any positive siderophore signal in the present samples. The observed media interference may have masked weak signals. Future testing should include three or more biological replicates and a positive control strain known to secrete siderophores under iron-limiting conditions, to better validate assay performance.

Ferric chloride assay results showed variable responses across strains and media. Although all DXM values were negative after media correction, relative comparisons suggest differences in apparent siderophore activity. Two-way ANOVA confirmed significant effects of strain ($p = 0.0003$), medium type ($p = 0.0021$), and their interaction ($p = 0.0006$). Within each strain one-way ANOVA tests revealed significant medium-dependent variation for all three strains: 4624 ($p = 0.022$), 7349 ($p = 0.028$), and 623 ($p = 0.004$).

For strain 4624, the DIP condition produced significantly less negative values than Fe or noFe, indicating stronger colour formation and a positive response to iron limitation. In contrast, 7349 showed the opposite pattern, with DIP samples being more negative—suggesting re-

Table 9: The table shows the results from the Ferric chloride test performed on all 24 hour samples. The values are shown in equivalents of desferrioxamine mesylate (DXM), calculated using the calibration curve in Figure 5.

		DXM equivalents			
Strain	Fermentation	Rep A	Rep B	Mean	St.dev
7349	Fe	-97.333	-96.900	-97.117	0.217
7349	noFe	-102.833	-99.867	-101.350	1.483
7349	DIP	-105.767	-104.700	-105.233	0.533
4624	Fe	-66.400	-72.200	-69.300	2.900
4624	noFe	-63.567	-63.333	-63.450	0.117
4624	DIP	-59.967	-61.200	-60.583	0.617
623	Fe	-83.300	-80.500	-81.900	1.400
623	noFe	-91.633	-89.367	-90.500	1.133
623	DIP	-108.433	-109.067	-108.750	0.317

duced complex formation despite statistical significance. Strain 623 presented a clear trend (Fe > noFe > DIP), but in the direction opposite of expected for siderophore activity, possibly reflecting assay interference or true suppression. As with the CAS assay, strong media interaction may have skewed absolute readings, limiting the assay's reliability for quantification. Still, comparative differences, especially for strain 4624, suggest potential siderophore secretion under DIP-induced iron stress.

A.2.3 Arnow and Rioux

Arnow assays were performed and DHBA equivalents were calculated using the calibration curved summarised below (Table 10) Arnow assay readings were used to assess catecholate-type siderophore activity across strains and media. Two-way ANOVA revealed highly significant effects of strain identity ($p = 1 \times 10^{-6}$), medium composition ($p = 8 \times 10^{-6}$), and their interaction ($p = 1 \times 10^{-6}$), supporting strong context-dependent variability.

Strain 4624 exhibited a markedly elevated response under DIP conditions, reaching over 0.04 mM 2,3-DHBA equivalents, an order of magnitude above any other sample. One-way ANOVA

Table 10: The slope, intercept and R^2 values from all calibration curves for the Arnow assay is depicted. The Arnow assay was used to test all the strains for catecholates, then on all the hourly fermentations samples taken form the 4624 DIP A fermentation. The last Arnow run was performed on the XAD-2 purification effluents.

	Slope	Intercept	R^2
All strains tested	3.0017	0.0022	0.9999
In DIP-4624 VS time	2.9230	-0.0027	1.0000
XAD-2 purification	2.7779	-0.0610	0.9999

confirmed this increase as statistically significant ($p = 0.0007$), and Tukey's HSD showed DIP $>$ Fe ($p = 0.004$) and DIP $>$ noFe ($p = 0.006$), while Fe and noFe were not significantly different. In contrast, neither 7349 nor 623 showed significant changes across media (p = 0.98 and 0.17, respectively), with all values near assay baseline.

These findings support strong catechol production by 4624 under DIP-induced iron limitation, while the other strains remained negative for catecholate siderophores under the tested conditions.

Table 11: The table shows the results from the Arnow assay performed on all 24 hour samples. The values are shown in equivalents of 2,3-dihydroxybenzoic acid (DHBA) calculated from the calibration curve in Figure 6.

		DHBA equivalents			
Strain	Fermentation	Rep A	Rep B	Mean	St.dev
7349	Fe	0.0029	0.0018	0.0024	0.0005
7349	noFe	0.0023	0.0023	0.0023	0.0000
7349	DIP	0.0024	0.0021	0.0022	0.0001
4624	Fe	0.0025	0.0013	0.0019	0.0006
4624	noFe	0.0066	0.0062	0.0064	0.0002
4624	DIP	0.0440	0.0351	0.0396	0.0044
623	Fe	0.0021	0.0009	0.0015	0.0006
623	noFe	0.0021	0.0026	0.0024	0.0002
623	DIP	0.0011	0.0002	0.0007	0.0005

Rioux assay results suggest strain- and media-specific variation in catecholate-type siderophore activity, though the reliability of the data is limited. The assay showed poor reproducibility between replicates and saturation effects in some samples, with absorbances approaching or exceeding spectrophotometer limits. Even for water samples in assay had high absorbances, raising concerns about baseline interference.

Table 12: The table shows the results from the Rioux assay performed on all 24 hour samples. The values are shown in equivalents of 2,3-dihydroxybenzoic acid (DHBA), calculated from the calibration curve in Figure 7.

		DHBA equivalents			
Strain	Fermentation	Rep A	Rep B	Mean	St.dev
7349	Fe	0.052	0.045	0.049	0.003
7349	noFe	0.045	0.076	0.060	0.015
7349	DIP	0.019	0.056	0.038	0.018
4624	Fe	0.042	0.069	0.056	0.013
4624	noFe	0.037	0.067	0.052	0.015
4624	DIP	0.081	0.085	0.083	0.002
623	Fe	0.023	0.046	0.035	0.012
623	noFe	0.014	0.038	0.026	0.012
623	DIP	0.009	0.029	0.019	0.010

Despite this, two-way ANOVA revealed significant effects for strain ($p = 0.004$), medium ($p = 0.009$), and their interaction ($p = 0.002$). Analysis within strains highlighted a significant increase in 4624 under DIP conditions ($p = 0.014$), with Tukey HSD confirming DIP $>$ Fe and DIP $>$ noFe. In contrast, neither 7349 ($p = 0.37$) nor 623 ($p = 0.19$) showed statistically significant variation, despite 623 displaying a decreasing trend from Fe to DIP. The large discrepancy between duplicates in 7349 (e.g., DIP A = 0.019, B = 0.056, see Figure 12) further exemplified the variance and undermined the statistical power of the Rioux assay results.

Overall, while the Rioux assay tentatively supports increased catecholate activity in 4624 under iron limitation, its limited reproducibility makes it less reliable for definitive conclusions.

A.2.4 Csaky and Atkin assay

Csaky assay values were consistently negative across all samples after normalising based on media interference. This suggests substantial interference from media components, likely masking any true signal from hydroxamate-type siderophores. As with the CAS assay, the data should be interpreted as comparative rather than quantitative.

Table 13: The table shows the results from the Csaky assay performed on all 24 hour samples. The values are shown in equivalents of desferrioxamine mesylate (DXM), calculated from the calibration curve in Figure 8.

		DXM equivalents			
Strain	Fermentation	Rep A	Rep B	Mean	St.dev
7349	Fe	-6.150	-4.150	-5.150	1.000
7349	noFe	-6.150	-5.900	-6.025	0.125
7349	DIP	-0.900	-3.150	-2.025	1.125
4624	Fe	-3.150	-2.400	-2.775	0.375
4624	noFe	-3.150	-3.900	-3.525	0.375
4624	DIP	-2.150	1.350	-0.400	1.750
623	Fe	-3.650	-1.650	-2.650	1.000
623	noFe	-4.150	-4.650	-4.400	0.250
623	DIP	-0.400	-2.400	-1.400	1.000

Despite this limitation, the two-way ANOVA still revealed significant effects for strain ($p = 0.018$), media ($p = 0.0030$), and their interaction ($p = 0.016$). Within-strain analysis showed that 4624 had a significantly higher hydroxamate signal in DIP compared to both Fe and noFe conditions (Tukey: DIP $>$ noFe, $p = 0.039$; DIP $>$ Fe, $p = 0.048$). This may indicate weak hydroxamate production under DIP-induced iron limitation. Strains 7349 and 623 showed similar directional trends, with DIP values closer to zero, but these did not reach full statistical significance. For 623, DIP differed significantly from noFe ($p = 0.042$) but not from Fe. Overall, the data hint at weak hydroxamate-related activity in 4624 under DIP conditions but remain inconclusive due to assay variability and potential matrix effects.

Atkin assay values showed minimal interference from media components, suggesting the results are more reliable and possibly quantitative. While no comparisons within strains reached statistical significance (all $p > 0.1$), the two-way ANOVA revealed significant effects of both strain ($p = 0.009$) and medium ($p = 0.013$), though not their interaction ($p = 0.50$).

All three strains followed a similar directional trend where DIP $>$ Fe $>$ noFe, with 7349 showing the clearest shift. This suggests a weak but consistent hydroxamate response under iron-limited conditions—most evident in 7349, although still below significance with $n = 2$. These findings reinforce the need for replicate expansion to confirm strain-specific siderophore secretion patterns.

Table 14: The table shows the results from the Atkin assay performed on all 24 hour samples. The values are shown in equivalents of desferrioxamine mesylate (DXM), calculated from the calibration curve in Figure 9.

		DXM equivalents			
Strain	Fermentation	Rep A	Rep B	Mean	St.dev
7349	Fe	17.667	9.833	13.750	3.917
7349	noFe	6.167	6.750	6.458	0.292
7349	DIP	15.333	22.083	18.708	3.375
4624	Fe	16.333	9.250	12.792	3.542
4624	noFe	9.333	8.000	8.667	0.667
4624	DIP	22.250	15.167	18.708	3.542
623	Fe	4.167	7.750	5.958	1.792
623	noFe	6.000	1.667	3.833	2.167
623	DIP	8.833	4.417	6.625	2.208

A.2.5 Tetrazolium test

The Tetrazolium assay for hydroxamate detection was carried out in 0.5 mL sample volumes within Eppendorf tubes. Upon reagent addition, the assay mixtures developed a visible precipitate, rendering spectrophotometric quantification unfeasible. As a result, all assessments were made visually, with colour development compared against known controls: 2,3-dihydroxybenzoic acid (DHBA), desferrioxamine mesylate (DXM), and Milli-Q water.

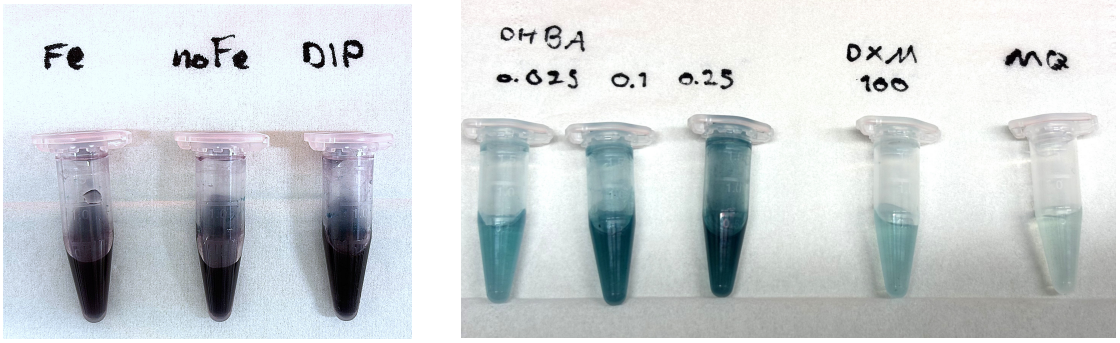

(a) Unused media samples of the Fe, noFe and DIP media. They all had a purple colour development.

(b) Siderophore standards and control sample with milli-Q water was tested with. 2,3-Dihydroxybenzoic acid (DHBA) was applied in concentrations 0.025, 0.1 and 0.25 mM, while desferrioxamine mesylate (DXM) was tested at 100 μM.

Figure 14: Media controls and siderophore reference samples from the Tetrazolium test. The colour developments were used to visually evaluate the fermentation samples.

As illustrated in Figure 14, Milli-Q water served as a negative control and produced only a faint blue hue. DHBA, although primarily a catecholate, showed a pronounced turquoise-blue colour at higher concentrations, while DXM generated a similar visual response. Despite this cross-reactivity with catecholates, the Tetrazolium assay is typically regarded as selective for hydroxamates, and the blue-turquoise colour seen in the standards served as a reference for identifying positive reactions. Notably, all media-only controls exhibited a deep purple colour with reddish undertones, distinct from the blue spectrum indicative of hydroxamate presence. This colour development appeared to result from media components themselves and complicated interpretation of the sample results.

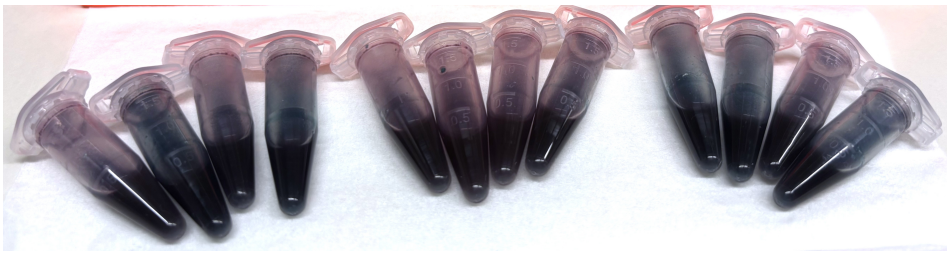

(a) 4624 fermentation samples samples. From left to right they are Fe A 9h and 24h, Fe B 9h and 24h, noFe A 9h and 24h, noFe B 9h and 24h, DIP A 11h and 24h, and DIP B 11h and 24h.

(b) 7349 fermentation samples samples. From left to right they are Fe A 12h and 24h, Fe B 12h and 24h, noFe A 12h and 24h, noFe B 12h and 24h, DIP A 11h and 24h, and DIP B 11h and 24h.

(c) 623 fermentation samples samples. From left to right they are Fe A 9h and 24h, Fe B 9h and 24h, noFe A 9h and 24h, noFe B 9h and 24h, DIP A 9h and 24h, and DIP B 9h and 24h.

Figure 15: The three pictures show the result of the Tetrazolium test for hydroxamate type siderophores on the fermentation samples. A purple with red under-tones indicate a negative result, while samples showing a more blue colour are positive results.

As shown in Figure 15, all 4624 and 623 samples developed a similarly deep purple colour to that of the media controls, suggesting a negative result for hydroxamates. The 4624 DIP samples showed a slight blue tinge beneath the dominant purple, possibly hinting at a weak or obscured reaction, though not conclusively positive. 7349 and its controls also produced a purple hue; however, the 7349 DIP A and B samples at 24 hours stood out by developing a distinctly turquoise-blue colour. These were the only samples classified as definitively positive for hydroxamate-type siderophores in this assay.

A.2.6 Shenker's assay

All samples were scanned in triplicates on the spectrum of 200 to 280 nm, giving a spectrum. From each sample spectrum, four peaks were isolated, each within these intervals; 229-233, 244-249, 259-263, and 269-273 nm. Each peak was analysed separately and compared with the corresponding peak in all the samples, looking for patterns. The tables below show the data fro each of the peaks

Unfortunately no media controls were run in this assay making the possible media interference unknown. As a consequence, though it may look as though the DIP fermentations are emitting a different absorbance than Fe and noFe, this difference is consistent across all the four peaks and for all the fermentation conditions. The overall conclusion is that none of the strains show a clear production of carboxylate type siderophores.

Table 15: The table shows the results from the Shenker assay performed on all 24 hour samples. The values are shown as the absorbance of the peak identified between 229 and 233 nm of the spectra.

		Absorbance at 229-233 nm peak			
Strain	Fermentation	Rep A	Rep B	Mean	St.dev
7349	Fe	0.050	0.047	0.049	0.002
7349	noFe	0.024	0.032	0.028	0.004
7349	DIP	0.100	0.118	0.109	0.009
4624	Fe	0.062	0.037	0.049	0.013
4624	noFe	0.044	0.045	0.045	0.001
4624	DIP	0.098	0.089	0.093	0.005
623	Fe	0.047	0.035	0.041	0.006
623	noFe	0.041	0.038	0.039	0.001
623	DIP	0.077	0.077	0.077	0.000

Table 16: The table shows the results from the Shenker assay performed on all 24 hour samples. The values are shown as the absorbance of the peak identified between 244 and 249 nm of the spectra.

		Absorbance at 244-249 nm peak			
Strain	Fermentation	Rep A	Rep B	Mean	St.dev
7349	Fe	0.055	0.049	0.052	0.003
7349	noFe	0.023	0.029	0.026	0.003
7349	DIP	0.098	0.134	0.116	0.018
4624	Fe	0.063	0.046	0.055	0.009
4624	noFe	0.046	0.059	0.052	0.007
4624	DIP	0.113	0.110	0.111	0.002
623	Fe	0.041	0.046	0.044	0.002
623	noFe	0.051	0.033	0.042	0.009
623	DIP	0.078	0.084	0.081	0.003

Table 17: The table shows the results from the Shenker assay performed on all 24 hour samples. The values are shown as the absorbance of the peak identified between 259 and 263 nm of the spectra.

		Absorbance at 259-263 nm peak			
Strain	Fermentation	Rep A	Rep B	Mean	St.dev
7349	Fe	0.066	0.059	0.063	0.003
7349	noFe	0.050	0.036	0.043	0.007
7349	DIP	0.113	0.128	0.121	0.007
4624	Fe	0.091	0.061	0.076	0.015
4624	noFe	0.054	0.068	0.061	0.007
4624	DIP	0.115	0.124	0.119	0.005
623	Fe	0.055	0.049	0.052	0.003
623	noFe	0.044	0.052	0.048	0.004
623	DIP	0.087	0.099	0.093	0.006

Table 18: The table shows the results from the Shenker assay performed on all 24 hour samples. The values are shown as the absorbance of the peak identified between 269 and 273 nm of the spectra.

		Absorbance at 269-273 nm peak			
Strain	Fermentation	Rep A	Rep B	Mean	St.dev
7349	Fe	0.060	0.057	0.058	0.002
7349	noFe	0.036	0.042	0.039	0.003
7349	DIP	0.105	0.134	0.119	0.014
4624	Fe	0.063	0.049	0.056	0.007
4624	noFe	0.056	0.060	0.058	0.002
4624	DIP	0.126	0.127	0.127	0.000
623	Fe	0.059	0.049	0.054	0.005
623	noFe	0.050	0.040	0.045	0.005
623	DIP	0.083	0.093	0.088	0.005

A.2.7 Catecholate investigation of strain 4624

Glucose metabolism in 4624 was tracked by ion chromatography (Figure 16). All fermentations showed progressive glucose depletion, confirming active metabolism. Differences between conditions were minimal and consistent with the OD-based growth curves (Figure 13).

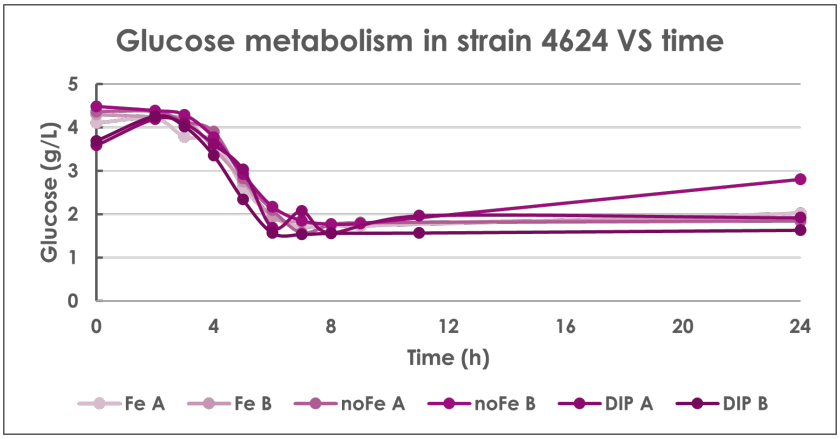

Figure 16: Glucose concentration in 4624 fermentations over 24 hours under different iron conditions. Glucose depletion patterns are shown for Fe, noFe, and DIP media. All cultures exhibit rapid consumption during early exponential growth, with DIP cultures showing slightly faster depletion. Measurements were made using ion chromatography. Data reflect duplicate fermentations per condition.

Catecholate levels in strain 4624 were measured throughout the fermentation using the Arnow assay, with values expressed as 2,3-dihydroxybenzoic acid (DHBA) equivalents. Standard curve details are provided in Table 10. Minimal catecholate production was observed in iron-rich (Fe) conditions, while noFe fermentations showed only a modest increase. In contrast, DIP cultures exhibited a sharp, early increase in catecholate secretion, plateauing after approximately 6 hours, indicating strong induction of siderophore biosynthesis under iron-chelating conditions. This rise coincided with the period of most rapid glucose consumption (see Figure 16), suggesting a link between metabolic activity and siderophore production.

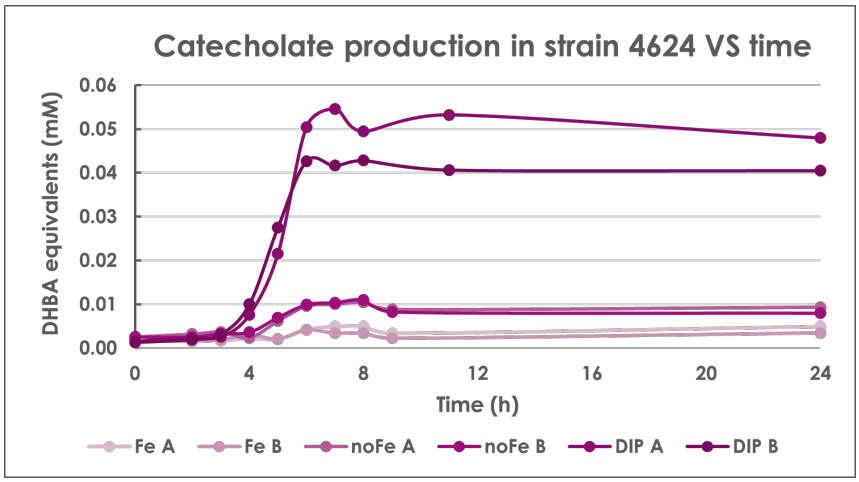

Figure 17: Catecholate production in strain 4624 during fermentation under different iron conditions.